Emerging trends in global freshwater availability

M. Rodell[1]*, J. S. Famiglietti[2,5], D. N. Wiese[2], J. T. Reager[2], H. K. Beaudoing[1,3], F. W. Landerer[2] & M.-H. Lo[4]

Freshwater availability is changing worldwide. Here we quantify 34 trends in terrestrial water storage observed by the Gravity Recovery and Climate Experiment (GRACE) satellites during 2002–2016 and categorize their drivers as natural interannual variability, unsustainable groundwater consumption, climate change or combinations thereof. Several of these trends had been lacking thorough investigation and attribution, including massive changes in northwestern China and the Okavango Delta. Others are consistent with climate model predictions. This observation–based assessment of how the world's water landscape is responding to human impacts and climate variations provides a blueprint for evaluating and predicting emerging threats to water and food security.

Groundwater, soil moisture, surface waters, snow and ice are dynamic components of the terrestrial water cycle[1–3]. Although they are not static on an annual basis (as early water-budget analyses supposed), in the absence of hydroclimatic shifts or substantial anthropogenic stresses they typically remain range-bound. Recent studies have identified locations where terrestrial water storage (TWS; the sum of these five components) appears to be trending below previous ranges, notably where ice sheets or glaciers are diminishing in response to climate change[4,5] and where groundwater is being withdrawn at an unsustainable rate[6–8].
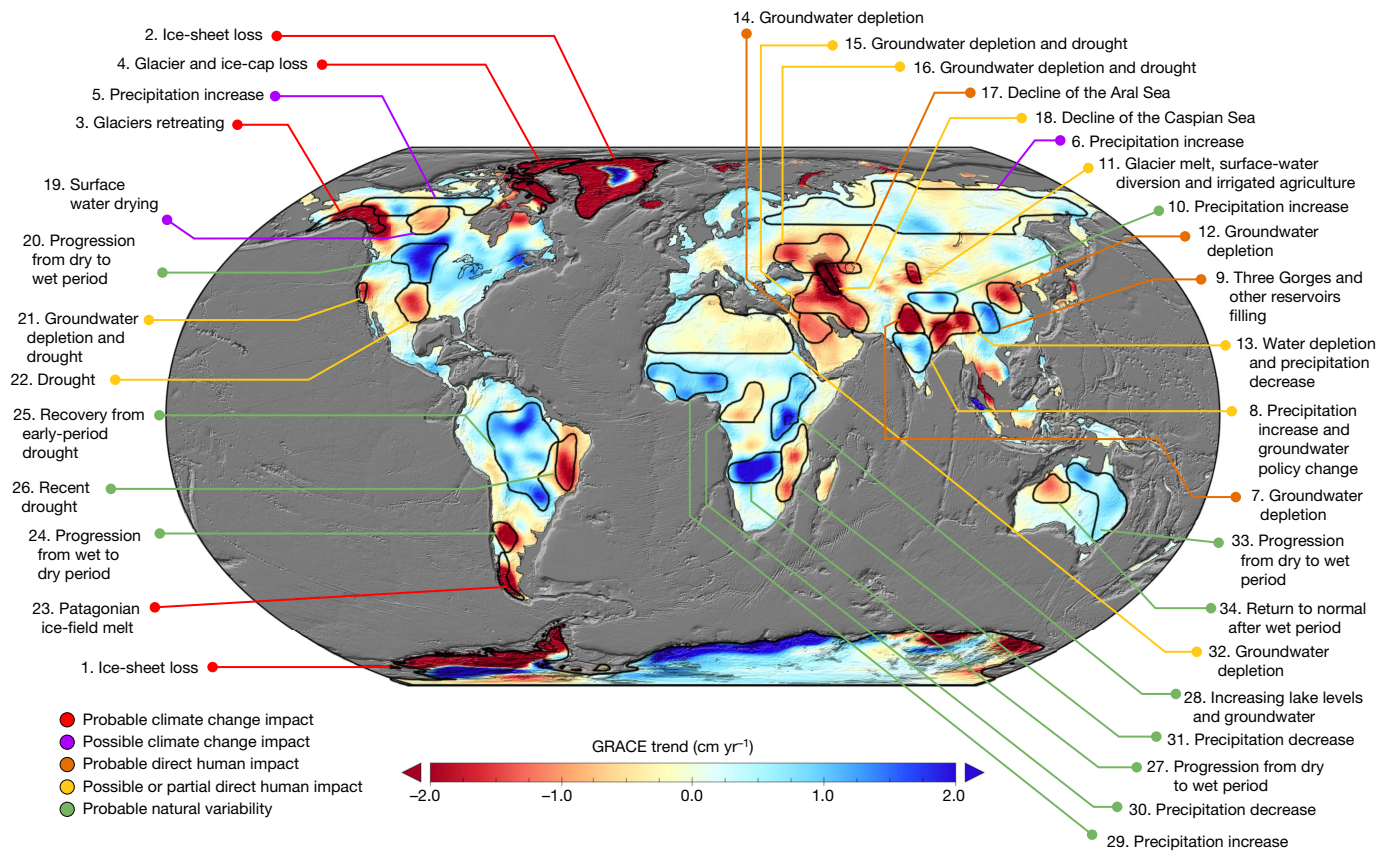
Accurate accounting of changes in freshwater availability is essential for predicting regional food supplies, human and ecosystem health, energy generation and social unrest. Groundwater is particularly difficult to monitor and manage because aquifers are vast and unseen, yet groundwater meets the domestic needs of roughly half of the world's population[9] and boosts food supply by providing for 38% of global consumptive irrigation water demand[10]. Nearly two-thirds of terrestrial aquatic habitats are being increasingly threatened[11], while the precipitation and river discharge that support them are becoming more variable[12]. A recent study[11] estimates that almost 5 billion people live in areas where threats to water security are likely—a situation that will only be exacerbated by climate change, population growth and human activities. Therefore, the key environmental challenge of the 21st century may be the globally sustainable management of water resources.

Much of our knowledge of past and current freshwater availability comes from a limited set of ground-based, point observations. Assessing changes in hydrologic conditions at the global scale is exceedingly difficult using in situ measurements alone, owing to the cost of installing and maintaining instrument networks, the presence of gaps in those networks and the lack of digitization and sharing of existing data[13]. Satellite remote sensing has proven crucial to monitoring water storage and fluxes in a changing world, enabling a truly global perspective that spans political boundaries[14]. In particular, since its launch in 2002, the GRACE mission[15] has tracked ice-sheet and glacier ablation, groundwater depletion and other TWS changes[16–19]. On a monthly basis GRACE can resolve TWS changes with sufficient accuracy over scales that range from approximately 200,000 km² at low latitudes to about 90,000 km² near the poles[1]. However, owing to GRACE's coarse spatial resolution, the inability to partition component mass changes and the brevity of the time series, proper

attribution of the TWS changes requires comprehensive examination of all available auxiliary information and data, which has never before been performed at the global scale.

Here we map TWS change rates around the globe based on 14 years (April 2002 – March 2016) of GRACE observations (Fig. 1). The GRACE data were processed using an advanced mass concentration[20] ('mascon') approach that enables improved signal resolution relative to the standard spherical-harmonic technique[21]. Best-fit linear rates of change after removing the seasonal cycle (referred to herein as 'apparent trends') are presented in Table 1 for 34 study regions. For context, the largest man-made reservoir in the USA, Lake Mead, has a capacity of about 32 Gt; during the study period, all but one of the 34 regions lost or gained more water than that, and eleven of them lost or gained more than ten times that amount. The reported uncertainty bounds are typically low because the process of removing glacial isostatic adjustment (GIA) signals is the only major source of error in the secular signal. Therefore, low uncertainty does not, on its own, imply that the apparent trends existed before the GRACE period or will continue into the future. The coefficient of determination (r^2), which represents the 'goodness of fit' of the regressed linear trends, is included in Table 1 to quantify the strength of the apparent trends relative to non-secular interannual variability. It is hence a useful, but by no means conclusive, piece of evidence that can be used to predict whether the trend will be fleeting or enduring, reflecting the cohesiveness of the TWS time series tendencies, as shown in Extended Data Fig. 1–4. We attribute the trends to natural variability, direct human impacts or climate change and forecast the likelihood that they will continue on the basis of 1979–2016 precipitation data from the Global Precipitation Climatology Project version 2.3 (GPCP)[22] (see Extended Data Figs. 5–8), an irrigated area map[23], satellite-based lake-level altimetry time series[24], Landsat imagery and published reports of human activities including agriculture, mining, reservoir operations and inter-basin water transfers. Further, for each region we provide the median climate model prediction of precipitation changes between 1986–2005 and 2081–2100 using the Representative Concentration Pathways 8.5 W m⁻² (RCP8.5; 8.5 W m⁻² radiative forcing in 2100 relative to pre-industrial levels) greenhouse gas emissions scenario from the Intergovernmental Panel on Climate Change (IPCC) Fifth Assessment Report[25]. We chose the high-end ('business as usual')

[1]Hydrological Sciences Laboratory, NASA Goddard Space Flight Center, Greenbelt, MD, USA. [2]Jet Propulsion Laboratory, California Institute of Technology, Pasadena, CA, USA. [3]Earth System Science Interdisciplinary Center, University of Maryland, College Park, MD, USA. [4]Department of Atmospheric Sciences, National Taiwan University, Taipei, Taiwan. [5]Present address: Global Institute for Water Security, School of Environment and Sustainability, and Department of Geography and Planning, University of Saskatchewan, Saskatoon, Canada. *e-mail: Matthew.Rodell@nasa.gov

2. Ice-sheet loss
4. Glacier and ice-cap loss
5. Precipitation increase
3. Glaciers retreating
19. Surface water drying
20. Progression from dry to wet period
21. Groundwater depletion and drought
22. Drought
25. Recovery from early-period drought
26. Recent drought
24. Progression from wet to dry period
23. Patagonian ice-field melt
1. Ice-sheet loss

14. Groundwater depletion
15. Groundwater depletion and drought
16. Groundwater depletion and drought
17. Decline of the Aral Sea
18. Decline of the Caspian Sea
6. Precipitation increase
11. Glacier melt, surface-water diversion and irrigated agriculture
10. Precipitation increase
12. Groundwater depletion
9. Three Gorges and other reservoirs filling
13. Water depletion and precipitation decrease
8. Precipitation increase and groundwater policy change
7. Groundwater depletion
33. Progression from dry to wet period
34. Return to normal after wet period
32. Groundwater depletion
28. Increasing lake levels and groundwater
31. Precipitation decrease
27. Progression from dry to wet period
30. Precipitation decrease
29. Precipitation increase

● Probable climate change impact
● Possible climate change impact
● Probable direct human impact
● Possible or partial direct human impact
● Probable natural variability

GRACE trend (cm yr^{-1})
−2.0 −1.0 0.0 1.0 2.0

Fig. 1 | Annotated map of TWS trends. Trends in TWS (in centimetres per year) obtained on the basis of GRACE observations from April 2002 to March 2016. The cause of the trend in each outlined study region is briefly explained and colour-coded by category. The trend map was smoothed with a 150-km-radius Gaussian filter for the purpose of visualization; however, all calculations were performed at the native 3° resolution of the data product.

scenario because it accentuates regional differences, which are more important for this analysis than absolute magnitudes are. Figure 2 presents maps of the IPCC, GPCP and irrigated-area data.

Global scale

By far the largest TWS trends occur in Antarctica (region 1; −127.6 ± 39.9 Gt yr^{-1} averaged over the continent), Greenland (region 2; −279.0 ± 23.2 Gt yr^{-1}), the Gulf of Alaska coast (region 3; −62.6 ± 8.2 Gt yr^{-1}) and the Canadian archipelago (region 4; −74.6 ± 4.1 Gt yr^{-1}), where the warming climate continues to drive rapid ice-sheet and glacier ablation[4,5,26,27]. Positive trends in sub-regions of Antarctica and Greenland result from increasing snow accumulation[28] and millennial-scale dynamic thickening processes[29,30]. Excluding those four ice-covered regions, one of the most striking aspects of changing TWS illuminated by Fig. 1 is that freshwater seems to be accumulating in far-northern North America (region 5) and Eurasia (region 6) and in the wet tropics, whereas the greatest non-frozen-freshwater losses have occurred at mid-latitudes[8,31]. The observed trends are consistent with increasing rates of northern high-latitude precipitation during the study period and with the prediction of IPCC models that precipitation generally will decrease in mid-latitudes and increase in low and high latitudes by the end of this century[25]. They also complement recent studies that identify increasing rates of precipitation in the tropics and increasing water storage and river discharge in the high Arctic[12,32]. However, because the rates of TWS change (0.45 ± 0.43 cm yr^{-1} and 0.17 ± 0.12 cm yr^{-1} in regions 5 and 6, respectively) and the coefficients of determination (0.52 and 0.10, correspondingly) are small, while GIA-related errors are relatively large, we cannot state definitively that these high-latitude tendencies are real trends.

A second characteristic of the map is that it reveals a clear 'human fingerprint' on the global water cycle. As seen in Fig. 2, freshwater is rapidly disappearing in many of the world's irrigated agricultural regions[6,10,33–38]. A third aspect of the global-trend map is natural inter-annual variability; many of the apparent trends are probably temporary, caused by oscillations between dry and wet periods (themselves driven by El Niño, La Niña and other climatic cycles) during the 14-year study period[39,40].

Eurasia

The hotspot in northern India (region 7) was among the first non-polar TWS trends to be revealed by GRACE[41,42]. It results from groundwater extraction to irrigate crops, including wheat and rice, in a semi-arid climate. Fifty-four per cent of the area is equipped for irrigation. We estimate the rate of TWS depletion to be 19.2 ± 1.1 Gt yr^{-1}, which is within the range of GRACE-based estimates from previous studies of differently defined northern-India regions[41–43]. The trend persists despite precipitation being 101% of normal (namely, the 1979–2015 GPCP annual mean for the region) during the study period, with an increasing trend of 15.8 mm yr^{-1}. The fact that extractions already exceed recharge during normal-precipitation years does not bode well for the availability of groundwater during future droughts. The contribution of Himalayan glacier mass loss to the regional trend is minor[41,42].

The increasing trend in central and southern India (region 8; 9.4 ± 0.6 Gt yr^{-1}) probably reflects natural variability of (mostly monsoon) rainfall, which was 104% of normal with an increasing rate of 3.7 mm yr^{-1} (0.4% per year). Although the r^2 value is low (0.24), the TWS and rainfall trends are both consistent with the RCP8.5-predicted 23% precipitation increase by 2100.

The increasing trend in eastern central China (region 9) is caused by a surge in dam construction and subsequent reservoir filling across that region[44]. The best known is the Three Gorges Dam reservoir, which was filled to its design capacity of 39.3 Gt between June 2003 and

Table 1 | TWS trends and supporting information

Region	Location	Area (km²)	TWS trend (Gt yr⁻¹)	TWS trend errors (Gt yr⁻¹)	r^2 of TWS trend	Irrigated area (%)	Precipitation trend (mm yr⁻¹)	Precipitation trend (% yr⁻¹)	Precipitation percentage of normal (%)	Predicted precipitation change (%)
1	Antarctica	12,397,401	−127.6	39.9	0.93	0	0.82	0.40	96.6	30.9
2	Greenland	2,184,307	−279.0	23.2	0.97	0	8.85	2.09	102.7	39.1
3	Gulf of Alaska coast	716,492	−62.6	8.2	0.93	0	−3.03	−0.25	95.0	21.3
4	Canadian Archipelago	672,413	−74.6	4.1	0.95	0	−5.33	−2.11	94.5	38.3
5	Northern North America	1,350,129	6.1	5.8	0.52	0	2.35	0.73	105.1	26.9
6	Northern Eurasia	8,009,175	13.4	9.7	0.10	0	1.65	0.30	104.4	25.1
7	Northern India	664,169	−19.2	1.1	0.80	54	15.80	2.20	101.0	11.8
8	Central India	1,352,670	9.4	0.6	0.24	51	3.72	0.36	103.7	23.1
9	Eastern Central China	657,375	7.8	1.6	0.78	14	7.33	0.77	99.6	7.9
10	Tibetan Plateau	881,704	7.7	1.4	0.67	0	−1.52	−0.90	104.2	19.7
11	Northwestern China	215,152	−5.5	0.5	0.77	7	1.11	0.57	109.8	15.3
12	North China Plain	876,004	−11.3	1.3	0.63	52	−2.33	−0.37	103.0	19.4
13	Eastern India Region	1,228,839	−23.3	1.9	0.85	25	−9.52	−0.67	96.1	14.7
14	Northwestern Saudi Arabia	841,763	−10.5	1.5	0.92	0	−1.44	−1.31	77.7	−1.4
15	Northern Middle East	2,189,561	−32.1	1.5	0.84	5	−2.80	−0.90	96.3	−8.5
16	Southwestern Russia Region	1,772,712	−18.1	1.3	0.64	15	−5.83	−0.92	96.8	6.2
17	Aral Sea	52,299	−2.2	0.1	0.76	0	2.71	1.17	111.1	5.9
18	Caspian Sea	377,761	−23.7	4.2	0.76	0	−4.37	−1.14	103.4	2.1
19	Central Canada	802,682	−7.0	6.4	0.73	0	0.69	0.17	102.0	16.9
20	Northern Great Plains	1,333,598	20.2	4.8	0.79	3	2.26	0.44	102.0	7.0
21	Southern California	177,996	−4.2	0.4	0.46	18	−8.31	−1.29	89.7	1.2
22	Southern High Plains and eastern Texas	1,105,113	−12.2	3.6	0.44	9	−5.71	−0.76	95.2	−2.8
23	Patagonian ice fields	461,198	−25.7	5.1	0.89	0	−8.01	−0.76	97.1	−6.9
24	Central Argentina[a]	530,661	−8.6	1.2	0.77	4	1.87	0.32	94.2	0.7
25	Central and western Brazil	5,559,805	51.9	9.4	0.39	1	0.61	0.03	100.2	−5.0
26	Eastern Brazil	1,132,450	−16.7	2.9	0.39	1	−16.97	−1.61	97.7	−5.9
27	Okavango Delta	1,589,692	29.5	3.5	0.55	0	−5.21	−0.61	105.3	−8.7
28	Nile headwaters	1,824,276	21.9	3.9	0.56	1	−3.53	−0.30	97.7	11.6
29	Tropical western Africa	2,298,134	24.1	2.1	0.67	1	−0.12	−0.01	103.4	−6.3
30	Northern Congo	1,318,261	−7.2	1.0	0.26	0	−1.55	−0.10	99.1	7.1
31	Southeastern Africa	1,677,719	−12.9	2.3	0.47	0	−3.23	−0.32	95.9	−5.9
32	Northern Africa	6,664,135	−11.7	2.9	0.45	1	−0.12	−0.19	106.7	−12.9
33	Northern & Eastern Australia	2,504,494	19.0	2.8	0.32	3	4.30	0.69	104.6	−6.0
34	Northwestern Australia	1,002,367	−8.9	1.2	0.43	0	−0.39	−0.10	99.1	−0.6

Location; area; GRACE-based TWS trend (April 2002–March 2016) and uncertainty; coefficient of determination (r^2) of the fitted linear trend; percentage of the area equipped for irrigation[23]; trend in precipitation[22] (January 2002–March 2016) after removing the seasonal cycle; annual mean precipitation (2003–2015) as a fraction of the long-term (1979–2015) annual mean[22]; and median precipitation change between the periods 1986–2005 and 2081–2100, predicted using the IPCC high-end greenhouse gas emissions scenario[25] for each of the 34 study regions.
[a]The TWS trend in region 24 is for April 2002–February 2010 only.

October 2010[45]. The 14-year regional trend, 7.8 ± 1.6 Gt y⁻¹r, did not change appreciably after the Three Gorges Dam Reservoir was filled. That can be explained by both the prevalence of other dam projects and the greater precipitation after 2010 (971 mm yr⁻¹; compared to 928 mm yr⁻¹ before 2010). Further, seepage from dams tends to raise the regional water table, which can continue for years before the system equilibrates[46]. If precipitation trends towards an 8% increase by the end of this century, as predicted, then the observed TWS trend may persist even after the current dam building boom, although probably at a slower pace.

Satellite altimetry and Landsat data indicate that the majority of lakes in the Tibetan Plateau have grown in water level and extent during the 2000s owing to a combination of elevated precipitation rates and increased glacier-melt flows[47], which are difficult to disentangle. From 1997 to 2001 the average annual precipitation in region 10 was 160 mm yr⁻¹, well below the 2002–2015 average of 175 mm yr⁻¹; thus, the observed increase in TWS (7.7 ± 1.4 Gt yr⁻¹) may reflect replenishment after a prolonged dry period. Additional surface-water storage would have been partially offset by glacier retreat and warming-enhanced evaporation. The GIA may further complicate the partitioning of the GRACE-derived mass-change signal over the Tibetan Plateau[48], but some have argued that the GIA contribution is negligible[49]. The latter study[49] noted that interannual mass variability in the region during the GRACE period is large relative to the inferred trend[49]. We concur ($r^2 = 0.67$) and conclude that there is no basis for extrapolating the apparent TWS trend into the future. In fact, it appears to have reversed in 2013 (Extended Data Fig. 2). Although RCP8.5

predicts a 20% increase in precipitation by 2100, it is probable that warming-induced glacier-mass losses will begin to exceed surface-water gains, particularly if the fraction of frozen precipitation decreases.

Region 11 lies to the west of the city of Urumqi in northwestern China's Xinjiang province. During the study period, TWS depletion was intense: -5.5 ± 0.5 Gt yr⁻¹ from an area of only 215,000 km². Precipitation data indicate that drought was a non-factor. The glaciers of the Tien Shan mountain range, whose central third lies within region 11, are melting rapidly[49], but not rapidly enough to explain all of the mass loss. Groundwater is being withdrawn to support irrigated agriculture across the province[50,51] and possibly to dewater coal mines[52]. However, region 11 is contained within an endorheic basin. Hence, the additional surface water produced by ice-melt and groundwater abstraction cannot flow far, yet the elevations of the five lakes within that basin either declined or were stable during the study period and GRACE did not detect substantial TWS increases in other parts of the basin. We conclude that region 11 is losing glacier ice and possibly groundwater, which ultimately become evapotranspiration, both in irrigated agricultural areas to the north, south and west of the mountains, as well as through evaporation from the desert floor to the south[50]. Details are provided in Methods.

The vast agricultural region surrounding Beijing (region 12) is heavily irrigated (52%). Previous GRACE-based studies offered a wide range of estimates for groundwater depletion from the North China Plain aquifer (see Methods for details), which is encompassed by region 12 and supports much of that irrigation. Here we estimate a TWS change rate of -11.3 ± 1.3 Gt yr⁻¹ for region 12. During the GRACE period,
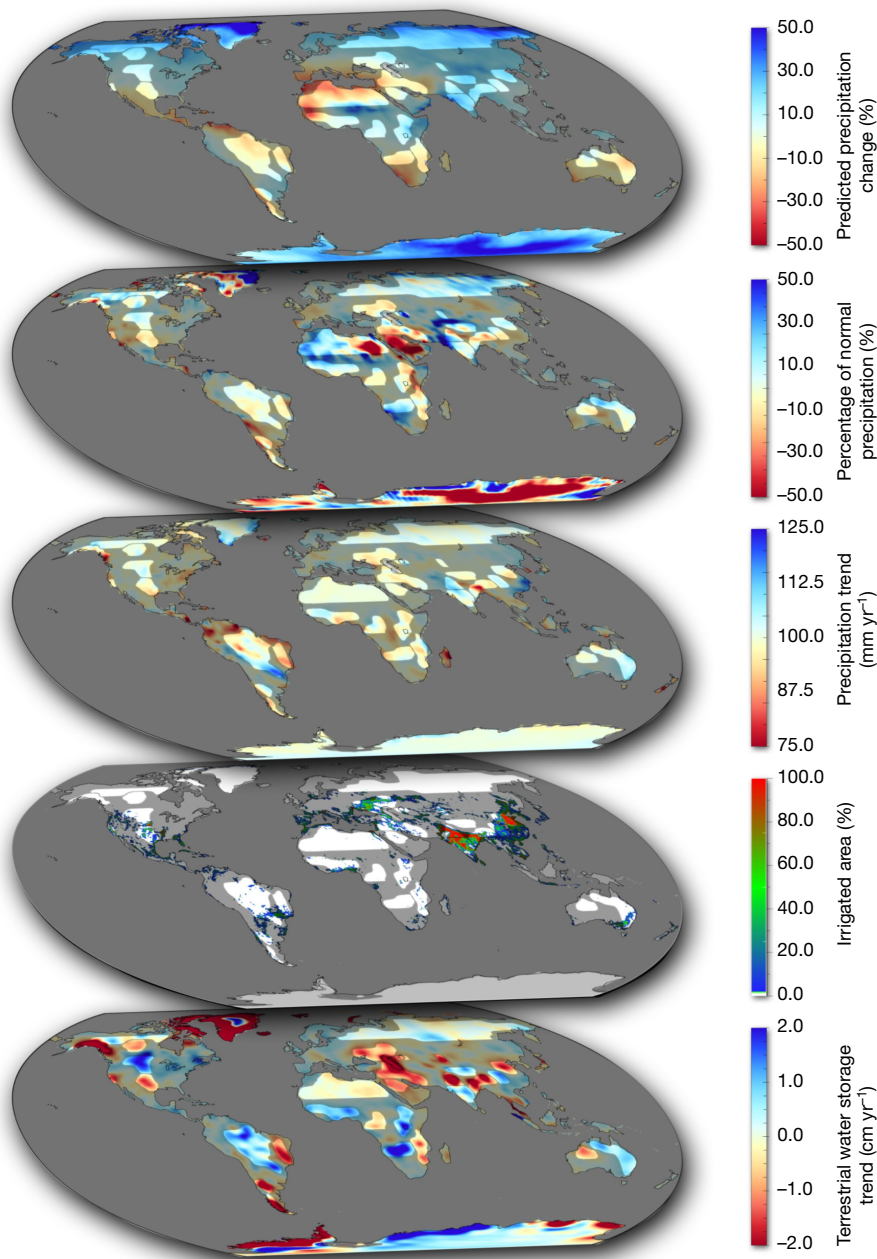
Fig. 2 | Trends in TWS and supporting data maps. (Bottom to top) TWS trends (in centimetres per year); percentage of area equipped for irrigation[23] (%); trend in precipitation[22] (in millimetres per year); mean annual precipitation (2003–2015) as a percentage of the long-term mean[22] (in per cent); IPCC-predicted change in precipitation[25] (in per cent). Areas outside of the study regions are shaded.

the total annual precipitation was steady at about 10 mm yr^{-1} above the 1979–2015 mean, following two dry years and a wet year during 2001–2003. All evidence suggests that this trend is human-induced and likely to continue until groundwater becomes scarce or regulations are put in place to reduce consumption rates.

The negative trend that extends across East India, Bangladesh, Burma and southern China (region 13), −23.3 ± 1.9 Gt yr^{-1}, may be explained by a combination of intense irrigation[53] (25%) and a decrease in monsoon season precipitation during the study period. The total annual precipitation was well above normal from 1998 to 2001, resulting in elevated TWS. During the GRACE period, precipitation declined at a rate of −10 mm yr^{-1} (−0.7% per year), and the annual accumulations were below average from 2009 to 2015. This is the third most heavily irrigated of the study regions, so TWS decline is likely to continue, although perhaps at a slower rate, given that rainfall should normalize eventually and a 15% increase in rainfall is predicted by 2100.

Decreasing water storage in the Middle East has been quantified using GRACE by previous studies[54–56]. Here we split the affected area into two regions, northwest Saudi Arabia (region 14; −10.5 ± 1.5 Gt yr^{-1}) and northern Middle East (region 15, which includes eastern Turkey, Syria, Iraq and Iran; −32.1 ± 1.5 Gt yr^{-1}). The declines result from a combination of recent drought and consequent increases in groundwater demand. Average precipitation during the study period was 78% and 96% of the 1979–2015 means in regions 14 and 15, respectively, with a slightly declining trend (−1% per year) in both. Although the irrigation dataset indicates that less than 1% of region 14 is irrigated, Landsat imagery reveals the appearance and expansion of crop irrigation over the past three decades, supplied by non-renewable groundwater. However, the Saudi Arabian government ended their domestic wheat production programme in market year 2014–15[57]. Thus, although some farms have continued to operate, it is likely that the depletion rate in region 14 will diminish, and TWS may already be stabilizing (Extended Data Fig. 2).

Region 15 has experienced a more complicated recent water history[54,58]. Turkey's construction of 22 dams upstream on the Tigris and Euphrates Rivers in the last three decades has considerably decreased the rate of flow into Iraq and Syria. Combined with long-term drought, this has forced widespread over-reliance on groundwater for both domestic and agricultural needs, and largely explains the large negative TWS trend[54,59]. Surface and groundwater depletion is likely to continue in a stepwise fashion, with periods of near-stability during normal-to-wet years and rapid declines during drought years.

To the north, an adjoining zone of TWS depletion (region 16; -18.1 ± 1.3 Gt yr^{-1}) extends from the Ukraine through western Russia and into Kazakhstan. As before, the root cause of this depletion is competition for scarce water resources, exacerbated by drought. Fifteen per cent of the area is irrigated, including fertile croplands that are vital to Russia. Precipitation during the study period was 97% of normal, with a decreasing trend of 6 mm yr^{-1} (1% per year). As in region 15, surface- and groundwater depletion in region 16 is likely to continue as it has, stepwise, with substantial declines during drought years (2008, 2012 and 2014) and lesser recoveries in normal-to-wet years.

The water demands of regions 15 and 16 place severe pressure on the Aral and Caspian Seas[60] (regions 17 and 18, respectively). The demise of the Aral Sea is well known. Our estimate of the mass change in what remains of it is -2.2 ± 0.1 Gt yr^{-1}. Water level fluctuations in the Caspian Sea have previously been attributed to meteorological variability[8] and direct evaporation from the sea[61]. We find that the annual discharge from the Volga River explains 60% of the variance in the annual mean level of the Caspian Sea compared with 18% explained by evaporation from the sea. Interannual variations in Volga River discharge are nearly three times as large as interannual variations in evaporation, and the former are controlled by both precipitation changes and the water demands of crops, which cover 37% of the basin. Using crop-production data and other information, we establish that the -23.7 ± 4.2 Gt yr^{-1} change rate of the water mass in the Caspian Sea observed by GRACE was caused in part by diversions and direct withdrawals of water from the rivers that sustain it (see Methods for details), mirroring the circumstances that doomed the Aral Sea. Because the Caspian Sea contains about 78,000 Gt of water, at the current rate it will survive for three more millennia, but a receding shoreline could be an issue.

Three mass changes in Eurasia that are prominent in Fig. 1 are not associated with TWS at all. Crustal deformation accompanying the magnitude-9.1 Sumatra–Andaman earthquake of 2004 caused two of these mass changes, the dipole positive and negative trends in Sumatra and the Malay Peninsula, respectively[62]. The magnitude-9.0 Tohoku earthquake of 2011 caused the negative trend in Japan[63].

North America

Ongoing GIA processes centred near Hudson Bay, where the Laurentide ice sheet was thickest 20 to 95 thousand years ago, require a correction of the mass rates observed by GRACE of up to 5–6 cm yr^{-1} (equivalent height of water)[64,65]. However, GIA models are imperfect and thus there is large uncertainty in the apparent decreasing TWS trend in central Canada (region 19) and some evidence that it may reflect an overcorrection of GIA[66]. Nevertheless, here we estimate the rate to be -7.0 ± 6.4 Gt yr^{-1}. Loss of water would be consistent with a recent study that concluded that Canada's subarctic lakes are vulnerable to drying when snow cover declines and that recent bouts of drying may be unprecedented in the past 200 years[67]. On the other hand, precipitation was 102% of normal during the GRACE period, and a 17% increase is predicted by the end of the century.

The wetting trend in the northern Great Plains (region 20), 20.2 ± 4.8 Gt yr^{-1}, arises from a combination of deep drought during 2001–2003, which depressed water levels greatly at the start of the GRACE period, followed by nine of the next eleven years having greater-than-average precipitation, including flooding in 2010–2011[68]. The trend is likely to diminish over time, although a 7% increase in precipitation is predicted by 2100.

A historically severe drought centred in southern California (region 21) that began in 2007 (ignoring a wet 2010) and consequent increases in groundwater demand[69,70] conspired to diminish TWS at a rate of -4.2 ± 0.4 Gt yr^{-1}. Although atmospheric rivers replenished California's surface waters during 2016–2017 and policy changes have been enacted, it is doubtful that aquifer storage will recover completely without large usage reductions, in part because dewatering of aquifer materials can cause compaction of sediments, thus reducing aquifer capacity irrevocably[71]. In the Central Valley, which provides one-third of the vegetables and two-thirds of the fruits and nuts grown in the US, annual water demands for agriculture have exceeded renewable water resources since the early 20th century[71]. Groundwater well observations that extend back to 1962 suggest that each successive drought causes groundwater levels to step down to a new normal range without full recovery[71], as in regions 15 and 16. Declining winter snowpack in the Sierra Nevada Mountains, including a 500-year low in 2015[72], is a major concern because it is the main source of the region's surface-water supply and groundwater recharge.

Sporadic droughts[73] in region 22, which encompasses parts of the southern High Plains and Texas, produced an apparent trend of -12.2 ± 3.6 Gt yr^{-1} during the GRACE period. In this case we forecast partial replenishment. Large precipitation variations caused TWS to seesaw between high and low (Extended Data Fig. 7). Heavy rains that led to flooding in parts of Texas and Oklahoma in May 2015, October 2015 and June 2016 ended the most recent drought and reduced the linear rate of TWS decline during the GRACE period. On the other hand, withdrawals of groundwater to support irrigated agriculture that exceed recharge in the central and southern High Plains aquifer have persisted for decades[74] and will continue until the resource is exhausted or management policies change. The fringes of the aquifer have already run dry in places, and recent estimates predict that the southern High Plains aquifer could be depleted within 30 years[74]. Despite this situation, entrenched water rights are likely to preserve the status quo until the damage forces the hands of policymakers and stakeholders.

South America

Melting of the Patagonian ice fields (region 23) has previously been documented using altimetry[75] and GRACE[76]. On the basis of our analysis (see Methods for details), TWS loss is occurring at a rate of -25.7 ± 5.1 Gt yr^{-1}. In a warming world, melting of the Patagonian ice fields will continue until they are exhausted.

The magnitude-8.8 Maule (Chile) earthquake that occurred on 27 February 2010 is partly responsible for the apparent trend in Central Argentina[77] (region 24). A model has not yet been developed to properly separate its effect from TWS variations after that date (Extended Data Fig. 3). TWS had previously been declining at a rate of -8.6 ± 1.2 Gt yr^{-1}. The region received substantially elevated precipitation in five of the six years between 1999 and 2004, producing a TWS surplus at the start of the GRACE period. Multi-year drought began in 2009, resulting in a negative trend observed from April 2002 to February 2010. TWS appears to have begun recovering (Extended Data Fig. 3) in response to above-normal precipitation in 2014 and 2015 (Extended Data Fig. 7), and we envisage that it will return to mean wetness conditions over time.

TWS increased during the GRACE period in central and western Brazil and its neighbours (region 25) at a rate of 51.9 ± 9.4 Gt yr^{-1}. The region received less-than-average rainfall in every year from 2001 to 2005, followed by greater-than-average rainfall in six of the next ten years. As a result, TWS recovered from the early-period drought[78] and exhibited a massive, but transitory, increasing trend which may have already ended (Extended Data Fig. 3). The magnitude of this trend is explained by both the size of the region and the intensity of the Amazon water cycle[79]. Still, we note that southern Brazil is a hotbed of dam construction[44], and it is possible that the filling of reservoirs contributed to the upward trend. Eastern Brazil (region 26) has recently suffered from a major drought[80], including well below normal rainfall in 2012, 2014 and 2015, causing TWS to plunge at a mean rate of -16.7 ± 2.9 Gt yr^{-1} during the GRACE period. In both cases, assuming precipitation rates revert towards (or oscillate around) their long-term means, the

observed trends should fade. In fact, owing to the recent strong El Niño, 2015 was the driest year in the 37-year record for region 25 (Extended Data Fig. 3), which may portend a reversion to average TWS.

Africa

Six apparent trends stand out in Africa. In southern Africa, a powerful wetting trend, 29.5 ± 3.5 Gt yr^{-1}, is observed in the western Zambezi basin, the Okavango delta and areas west of the coast (region 27). This region experienced a remarkable change in its hydroclimate. The area-averaged annual rainfall was less than 970 mm in every year from 1979 to 2005. That threshold was exceeded five times from 2006 to 2011. A permanent climatic shift was previously speculated on the basis of a significant decrease in annual precipitation in 1950–1975 and 1980–2005[81]. With ten years of additional hindsight, it appears that the region may have simply endured a prolonged drought from the late 1970s to the early 2000s. Thus, we attribute the GRACE-period trend to natural variability[82]. Although TWS appears to have peaked in 2012 (Extended Data Fig. 4), considering that the previous wet and dry periods lasted upwards of 25 years, it is plausible that the wetting trend could resume.

An apparent trend of 21.9 ± 3.9 Gt yr^{-1} occurs along the headwaters of the White Nile and Blue Nile rivers, including lakes Tanganyika and Victoria (region 28). Altimetry data indicate that during the study period both lakes experienced minimum water levels in 2006 and that their annual mean levels increased by 62 mm yr^{-1} and 40 mm yr^{-1} on average, respectively; these observations are consistent with the TWS time series. Together, the two lake level trends equate to less than a quarter (4.8 Gt yr^{-1}) of the observed TWS trend. Considering that, rainfall would seem to be the primary driver of TWS variations, while management of the large lakes[83] and dam building in the northern part of the region[84] also contribute. However, rainfall is not particularly well correlated with either TWS or lake levels. The lack of correlation may be indicative of inaccuracies stemming from the sparsity of rain gauges in the region. The observed rainfall trend was negligible during the study period, but a 12% increase is predicted by 2100. The northern part of region 28 encompasses the Grand Ethiopian Renaissance Dam on the Blue Nile River at Ethiopia's northwest border with Sudan, which Egypt has strongly denounced because of the possibility of reduced flow through the Nile. Construction of the dam began in 2011 and is ongoing. Filling of the 74-km^3 reservoir will probably produce a temporary increasing TWS trend in its immediate vicinity.

TWS has been increasing in tropical western Africa (region 29) at a rate of 24.1 ± 2.1 Gt yr^{-1}. Precipitation was 3% below normal in 2000–2002 and 3% above normal during the rest of the GRACE period. This appears to be the primary cause of TWS accumulation, although the possible contribution of the many dams being built in this part of Africa[44] is unknown. Because interannual variability of rainfall is substantial in the region[85], disregarding the dams it is likely that the change rate of TWS will oscillate around zero over the coming decades. By 2100, rainfall is predicted to decrease by 6%; hence, the dam construction may be timely.

Decreasing TWS (-7.2 ± 1.0 Gt yr^{-1}) in region 30, which extends from the coast of central Africa into the northern Congo River basin, seems to be caused by natural interannual variability, although it has been suggested that the surface runoff rate has been enhanced by deforestation[84]. Between 1999 and 2002 rainfall averaged 4% above normal, while it averaged 1% below normal during the rest of the GRACE period, including two very dry years in 2014 and 2015. The decrease in TWS is also consistent with the postulated negative correlation between TWS in the Amazon and Congo basins[86], which further implicates large-scale climatic oscillation as the ultimate driver[85].

The negative trend along the coast of southeastern Africa (region 31), -12.9 ± 2.3 Gt yr^{-1}, reflects a recent severe drought[79], which has caused major food shortages. Rainfall was 4% below average during the GRACE period, including annual accumulations that were below normal in five of the last eight years and barely above normal in the other three. Water levels in Lake Malawi, which is in the centre of the

region, are well correlated with regional TWS. The lake declined at a mean rate of 78 mm yr^{-1} during the period, accounting for 2.3 Gt yr^{-1} of the observed TWS trend. Hence, it is likely that the apparent trend is primarily caused by natural variability[84], although a 6% decrease in rainfall is predicted during this century.

A weak negative trend, -11.7 ± 2.9 Gt yr^{-1}, extends across arid Africa north of 19° N, excluding Morocco (region 32). The coefficient of determination is not large at 0.45; nevertheless, precipitation during the GRACE period was 7% above normal, which suggests that the consumptive use of fossil groundwater to stimulate agriculture and economic development is the cause[55,84,87]. Three studies[6,10,36] estimated recent rates of consumptive groundwater use across North Africa to be 7.8 Gt yr^{-1}, 15.7 Gt yr^{-1} and 4.1 Gt yr^{-1}, bracketing our TWS depletion estimate.

Australia

Australia appears to be bipolar with respect to water storage during the GRACE era, with wetting in the east and north and drying in the northwest. The worst drought in over 100 years afflicted eastern Australia during 2001–2009[88]. It is likely that groundwater was more heavily consumed during that time to compensate for reduced availability of surface waters. Recovery from the drought began with heavy rains in 2010 and transitioned to severe flooding in 2011, with so much water stored on the continent in 2012 that the global mean sea level temporarily declined[89]. The shift from dry to wet conditions caused the apparent wetting trend in region 33, 19.0 ± 2.8 Gt yr^{-1}, but most of that water had already been shed by 2016 (Extended Data Fig. 4). Northern Western Australia received greater-than-normal rainfall during every year from 1997 to 2001, including the two wettest years in the GPCP record in 2000 and 2001. Thus, region 34 began 2002 near the maximum TWS capacity, and it gradually returned to average[90] (-8.9 ± 1.2 Gt yr^{-1}) with 99% of normal precipitation during the GRACE period. It is possible that aquifer dewatering associated with Pilbara's mining industry also contributed, but reliable data are not available to confirm and quantify that contribution. We can only justifiably conclude that natural variability is the primary explanation for both Australian trends.

Implications and discussion

GRACE has revealed considerable changes in freshwater resources occurring across the globe and has allowed them to be quantified at regional scales, unimpeded by sparse measurements or restrictive data-access policies. Some of these changes are manifestations of human water management that, before GRACE, were known only anecdotally, including TWS depletion in northern India, the North China Plain and the Middle East (regions 7, 12 and 14–16), or not at all, as in northwestern China (region 11). These changes portend a future in which already limited water resources will become even more precious. Others correlate well with global warming and predicted future precipitation changes, including worldwide ice-sheet and glacier melt (regions 1–4 and 23) and TWS increases in the northern high latitudes (regions 5–6). Apparent TWS trends in about one-third of the study regions represent partial cycles of longer-term interannual oscillations and may fade or reverse over the decades (see green dots in Fig. 1). Although we have made every effort to attribute the apparent trends properly, they will all require continued observation to better understand their causes and constrain their rates.

The GRACE data provide motivation for multilateral cooperation among nations, states and stakeholders, including development of transboundary water-sharing agreements, to balance competing demands and defuse potential conflict[33]. Government policies that incentivize water conservation could help to avert a 'tragedy of the commons' scenario, that is, opportunistic competition for groundwater outweighing the altruistic impulse to preserve the resource. Northern India, the North China Plain, the Middle East and the area surrounding the Caspian Sea are already on a perilous path, while California, in response to severe drought and alarming groundwater declines in the Central Valley, recently passed legislation to regulate groundwater consumption.

In many regions, crop irrigation on massive scales has been supported by unsustainable rates of groundwater abstraction[6,33–36,91]. In the face of aquifer depletion, population growth and climate change, water and food security will depend upon water-saving technologies and improved management and governance. The success of such an approach in arid Israel[92] proves that a comprehensive water conservation strategy can work, and there are encouraging signs in Saudi Arabia (as previously discussed) and parts of India[93]. Meanwhile, as China looks to improve living standards for its 1.38 billion residents, it will continue to face daunting water-management decisions, many of which are related to massive geoengineering and water-diversion projects that are likely to trigger political tensions.

The GRACE data also call attention to regions where continued monitoring will be essential for distinguishing, understanding and quantifying climate change impacts on the water cycle[94,95] and groundwater[96,97] in particular. This is important for two reasons. First, verification of emerging hydroclimatic trends, such as increasing northern high-latitude precipitation, would raise confidence in the ability of climate models to predict water-cycle consequences of climate change[98]. Second, a redistribution of freshwater from dry to wet regions, as has been forecast, could exacerbate disparities between the water 'haves' and 'have-nots' and associated political instability, migration and conflict. Most groundwater depletion is occurring within Earth's mid-latitudes, resulting in a positive drying feedback that is accelerating water losses and the severity of related socioeconomic issues[33].

New and future satellite remote-sensing missions that extend the long-term record of global hydrological observations will be essential for continued assessment of changing freshwater availability[99]. In particular, the GRACE Follow On mission (planned to launch in early 2018), while affording a small increase in spatial resolution and accuracy[100], will enable surveillance of the trends described here and improved disentanglement of natural TWS variability from hydroclimatic change. Awareness of changing freshwater availability (for example, Fig. 1) is the first step towards addressing the challenges discussed here through improved infrastructure, water use efficiency, lifestyle and water-management decisions and policy.

Online content

Any Methods, including any statements of data availability and Nature Research reporting summaries, along with any additional references and Source Data files, are available in the online version of the paper at https://doi.org/10.1038/s41586-018-0123-1.

1. Changnon, S.A. *Detecting Drought Conditions in Illinois*. Circular 169 (Illinois State Water Survey, 1987).
2. Rodell, M. & Famiglietti, J. S. An analysis of terrestrial water storage variations in Illinois with implications for the Gravity Recovery and Climate Experiment (GRACE). *Wat. Resour. Res.* **37**, 1327–1339 (2001).
3. Getirana, A., Kumar, S., Girotto, M. & Rodell, M. Rivers and floodplains as key components of global terrestrial water storage variability. *Geophys. Res. Lett.* **44**, 10359–10368 (2017).
4. Luthcke, S. B. et al. Antarctica, Greenland and Gulf of Alaska land ice evolution from an iterated GRACE global mascon solution. *J. Glaciol.* **59**, 613–631 (2013).
5. Velicogna, I., Sutterley, T. C. & van den Broeke, M. R. Regional acceleration in ice mass loss from Greenland and Antarctica using GRACE time-variable gravity data. *Geophys. Res. Lett.* **41**, 8130–8137 (2014).
6. Wada, Y., van Beek, L. P. H. & Bierkens, M. F. P. Nonsustainable groundwater sustaining irrigation: a global assessment. *Wat. Resour. Res.* **48**, W00L06 (2012).
7. Konikow, L. F. Contribution of global groundwater depletion since 1900 to sea-level rise. *Geophys. Res. Lett.* **38**, L17401 (2011).
8. van Dijk, A. I. J. M., Renzullo, L. J., Wada, Y. & Tregoning, P. A global water cycle reanalysis (2003–2012) merging satellite gravimetry and altimetry observations with a hydrological multi-model ensemble. *Hydrol. Earth Syst. Sci.* **18**, 2955–2973 (2014).
9. Zektser, I. S. & Everett, L. G. (eds) *Groundwater Resources of the World and Their Use* (UNESCO, Paris, 2004); http://unesdoc.unesco.org/images/0013/001344/134433e.pdf.
10. Siebert, S. et al. Groundwater use for irrigation – a global inventory. *Hydrol. Earth Syst. Sci.* **14**, 1863–1880 (2010).
11. Vörösmarty, C. J. et al. Global threats to human water security and river biodiversity. *Nature* **467**, 555–561 (2010).
12. Syed, T. H., Famiglietti, J. S., Chambers, D. P., Willis, J. K. & Hilburn, K. Satellite-based global-ocean mass balance estimates of interannual variability and emerging trends in continental freshwater discharge. *Proc. Natl Acad. Sci. USA* **107**, 17916–17921 (2010).
13. Rodell, M. et al. The observed state of the water cycle in the early 21st century. *J. Clim.* **28**, 8289–8318 (2015).
14. Famiglietti, J. S. et al. Satellites provide the big picture. *Science* **349**, 684–685 (2015).
15. Tapley, B. D., Bettadpur, S., Ries, J. C., Thompson, P. F. & Watkins, M. M. GRACE measurements of mass variability in the Earth system. *Science* **305**, 503–505 (2004).
16. Wahr, J., Molenaar, M. & Bryan, F. Time variability of the Earth's gravity field: hydrological and oceanic effects and their possible detection using GRACE. *J. Geophys. Res. Solid Earth* **103**, 30205–30229 (1998).
17. Rodell, M. & Famiglietti, J. S. Detectability of variations in continental water storage from satellite observations of the time dependent gravity field. *Wat. Resour. Res.* **35**, 2705–2723 (1999).
18. Swenson, S., Yeh, P. J. F., Wahr, J. & Famiglietti, J. A comparison of terrestrial water storage variations from GRACE with in situ measurements from Illinois. *Geophys. Res. Lett.* **33**, L16401 (2006).
19. Cazenave, A. & Chen, J. Time-variable gravity from space and present-day mass redistribution in the Earth system. *Earth Planet. Sci. Lett.* **298**, 263–274 (2010).
20. Rowlands, D. D. et al. Resolving mass flux at high spatial and temporal resolution using GRACE intersatellite measurements. *Geophys. Res. Lett.* **32**, L04310 (2005).
21. Watkins, M. M., Wiese, D. N., Yuan, D. N., Boening, C. & Landerer, F. W. Improved methods for observing Earth's time variable mass distribution with GRACE using spherical cap mascons. *J. Geophys. Res. Solid Earth* **120**, 2648–2671 (2015).
22. Adler, R. et al. *The New Version 2.3 of the Global Precipitation Climatology Project (GPCP) Monthly Analysis Product* http://eagle1.umd.edu/GPCP_ICDR/GPCP_Monthly.html (2016).
23. Salmon, J. M., Friedl, M. A., Frolking, S., Wisser, D. & Douglas, E. M. Global rain-fed, irrigated, and paddy croplands: a new high resolution map derived from remote sensing, crop inventories and climate data. *Int. J. Appl. Earth Obs. Geoinf.* **38**, 321–334 (2015).
24. Birkett, C., Reynolds, C., Beckley, B. & Doorn, B. in *Coastal altimetry* (eds Vignudelli, S. et al.) 19–50 (Springer, Berlin, 2011).
25. Oldenborgh, G. J. et al. (eds) in *Climate Change 2013: The Physical Science Basis* (eds Stocker, T. F. et al.) 1311–1393 (Cambridge Univ. Press, Cambridge, 2013); http://www.ipcc.ch/pdf/assessment-report/ar5/wg1/WG1AR5_AnnexI_FINAL.pdf.
26. Tamisiea, M. E., Leuliette, E. W., Davis, J. L. & Mitrovica, J. X. Constraining hydrological and cryospheric mass flux in southeastern Alaska using space-based gravity measurements. *Geophys. Res. Lett.* **32**, L20501 (2005).
27. Gardner, A. S. et al. Sharply increased mass loss from glaciers and ice caps in the Canadian Arctic Archipelago. *Nature* **473**, 357–360 (2011).
28. Boening, C., Lebsock, M., Landerer, F. & Stephens, G. Snowfall-driven mass change on the East Antarctic ice sheet. *Geophys. Res. Lett.* **39**, L21501 (2012).
29. Schlegel, N.-J. et al. Application of GRACE to the assessment of model-based estimates of monthly Greenland Ice Sheet mass balance (2003–2012). *Cryosphere* **10**, 1965–1989 (2016).
30. MacGregor, J. A. et al. Holocene deceleration of the Greenland Ice Sheet. *Science* **351**, 590–593 (2016).
31. Reager, J. T. et al. A decade of sea level rise slowed by climate-driven hydrology. *Science* **351**, 699–703 (2016).
32. Landerer, F. W., Dickey, J. O. & Güntner, A. Terrestrial water budget of the Eurasian pan-Arctic from GRACE satellite measurements during 2003–2009. *J. Geophys. Res. Atmos.* **115**, D23115 (2010).
33. Famiglietti, J. S. The global groundwater crisis. *Nat. Clim. Chang.* **4**, 945–948 (2014).
34. Gleeson, T., Wada, Y., Bierkens, M. F. & van Beek, L. P. Water balance of global aquifers revealed by groundwater footprint. *Nature* **488**, 197–200 (2012).
35. Richey, A. S. et al. Uncertainty in global groundwater storage estimates in a total groundwater stress framework. *Wat. Resour. Res.* **51**, 5198–5216 (2015).
36. Döll, P., Schmied, H. M., Schuh, C., Portmann, F. T. & Eicker, A. Global-scale assessment of groundwater depletion and related groundwater abstractions: Combining hydrological modeling with information from well observations and GRACE satellites. *Wat. Resour. Res.* **50**, 5698–5720 (2014).
37. Long, D. et al. Global analysis of spatiotemporal variability in merged total water storage changes using multiple GRACE products and global hydrological models. *Remote Sens. Environ.* **192**, 198–216 (2017).
38. Dalin, C., Wada, Y., Kastner, T. & Puma, M. J. Groundwater depletion embedded in international food trade. *Nature* **543**, 700–704 (2017).
39. Phillips, T., Nerem, R., Fox-Kemper, B., Famiglietti, J. & Rajagopalan, B. The influence of ENSO on global terrestrial water storage using GRACE. *Geophys. Res. Lett.* **39**, L16705 (2012).
40. Humphrey, V., Gudmundsson, L. & Seneviratne, S. I. Assessing global water storage variability from GRACE: trends, seasonal cycle, subseasonal anomalies and extremes. *Surv. Geophys.* **37**, 357–395 (2016).
41. Rodell, M., Velicogna, I. & Famiglietti, J. S. Satellite-based estimates of groundwater depletion in India. *Nature* **460**, 999–1002 (2009).

42. Tiwari, V. M., Wahr, J. & Swenson, S. Dwindling groundwater resources in northern India, from satellite gravity observations. *Geophys. Res. Lett.* **36**, L18401 (2009).
43. Panda, D. K. & Wahr, J. Spatiotemporal evolution of water storage changes in India from the updated GRACE-derived gravity records. *Wat. Resour. Res.* **52**, 135–149 (2016).
44. Zarfl, C., Lumsdon, A. E., Berlekamp, J., Tydecks, L. & Tockner, K. A global boom in hydropower dam construction. *Aquat. Sci.* **77**, 161–170 (2015).
45. Wang, X., de Linage, C., Famiglietti, J. & Zender, C. S. Gravity Recovery and Climate Experiment (GRACE) detection of water storage changes in the Three Gorges Reservoir of China and comparison with in situ measurements. *Wat. Resour. Res.* **47**, W12502 (2011).
46. Chao, B. F., Wu, Y. H. & Li, Y. S. Impact of artificial reservoir water impoundment on global sea level. *Science* **320**, 212–214 (2008).
47. Zhang, G., Xie, H., Kang, S., Yi, D. & Ackley, S. F. Monitoring lake level changes on the Tibetan Plateau using ICESat altimetry data (2003–2009). *Remote Sens. Environ.* **115**, 1733–1742 (2011).
48. Zhang, T. Y. & Jin, S. G. Estimate of glacial isostatic adjustment uplift rate in the Tibetan Plateau from GRACE and GIA models. *J. Geodyn.* **72**, 59–66 (2013).
49. Jacob, T., Wahr, J., Pfeffer, W. T. & Swenson, S. Recent contributions of glaciers and ice caps to sea level rise. *Nature* **482**, 514–518 (2012).
50. Guo, M., Wu, W., Zhou, X., Chen, Y. & Li, J. Investigation of the dramatic changes in lake level of the Bosten Lake in northwestern China. *Theor. Appl. Climatol.* **119**, 341–351 (2015).
51. Stone, R. For China and Kazakhstan, no meeting of the minds on water. *Science* **337**, 405–407 (2012).
52. Hao, Y. et al. The role of climate and human influences in the dry-up of the Jinci Springs, China. *J. Am. Water Resour. Assoc.* **45**, 1228–1237 (2009).
53. Shamsudduha, M., Taylor, R. G. & Longuevergne, L. Monitoring groundwater storage changes in the highly seasonal humid tropics: validation of GRACE measurements in the Bengal Basin. *Wat. Resour. Res.* **48**, W02508 (2012).
54. Voss, K. A. et al. Groundwater depletion in the Middle East from GRACE with implications for transboundary water management in the Tigris-Euphrates-Western Iran region. *Wat. Resour. Res.* **49**, 904–914 (2013).
55. Sultan, M., Ahmed, M., Wahr, J., Yan, E. & Emil, M. in *Remote Sensing of the Terrestrial Water Cycle* (eds Lakshmi, V. et al.) 349–366 (John Wiley & Sons, Hoboken, 2014).
56. Joodaki, G., Wahr, J. & Swenson, S. Estimating the human contribution to groundwater depletion in the Middle East, from GRACE data, land surface models, and well observations. *Wat. Resour. Res.* **50**, 2679–2692 (2014).
57. USDA Foreign Agricultural Service. *Saudi Arabia Grain and Feed Annual, Global Agricultural Information Network*. Report number SA1602 (US Department of Agriculture, 2016); http://gain.fas.usda.gov/Recent%20GAIN%20 Publications/Grain%20and%20Feed%20Annual_Riyadh_Saudi%20 Arabia_3-14-2016.pdf.
58. Becker, R. H. The stalled recovery of the Iraqi marshes. *Remote Sens.* **6**, 1260–1274 (2014).
59. Chao, N., Luo, Z., Wang, Z. & Jin, T. Retrieving groundwater depletion and drought in the Tigris–Euphrates basin between 2003 and 2015. Ground Water (2017).
60. Zmijewski, K. & Becker, R. Estimating the effects of anthropogenic modification on water balance in the Aral Sea watershed using GRACE: 2003–12. *Earth Interact.* **18**, 1–16 (2014).
61. Chen, J. L. et al. Long-term Caspian Sea level change. *Geophys. Res. Lett.* **44**, 6993–7001 (2017).
62. Han, S.-C., Sauber, J., Luthcke, S. B., Ji, C. & Pollitz, S. S. Implications of postseismic gravity change following the great 2004 Sumatra-Andaman earthquake from the regional harmonic analysis of GRACE intersatellite tracking data. *J. Geophys. Res. Solid Earth* **113**, B11413 (2008).
63. Han, S. C., Sauber, J. & Riva, R. Contribution of satellite gravimetry to understanding seismic source processes of the 2011 Tohoku-Oki earthquake. *Geophys. Res. Lett.* **38**, L24312 (2011).
64. Peltier, W. R., Argus, D. F. & Drummond, R. Space geodesy constrains ice age terminal deglaciation: the global ICE-6G_C (VM5a) model. *J. Geophys. Res. Solid Earth* **120**, 450–487 (2015).
65. Peltier, W. R., Argus, D. F. & Drummond, R. Comment on "An Assessment of the ICE-6G_C (VM5a) glacial isostatic adjustment model by Purcell et al. *J. Geophys. Res. Solid Earth* **122**, 2019–2028 (2017).
66. Forman, B. A., Reichle, R. H. & Rodell, M. Assimilation of terrestrial water storage from GRACE in a snow-dominated basin. *Wat. Resour. Res.* **48**, W01507 (2012).
67. Bouchard, F. et al. Vulnerability of shallow subarctic lakes to evaporate and desiccate when snowmelt runoff is low. *Geophys. Res. Lett.* **40**, 6112–6117 (2013).
68. Reager, J. T. et al. Assimilation of GRACE terrestrial water storage observations into a land surface model for the assessment of regional flood potential. *Remote Sens.* **7**, 14663–14679 (2015).
69. Famiglietti, J. S. et al. Satellites measure recent rates of groundwater depletion in California's Central Valley. *Geophys. Res. Lett.* **38**, L03403 (2011).
70. Scanlon, B. R. et al. Groundwater depletion and sustainability of irrigation in the US High Plains and Central Valley. *Proc. Natl Acad. Sci. USA* **109**, 9320–9325 (2012).
71. Faunt, C. C., Sneed, M., Traum, J. & Brandt, J. T. Water availability and land subsidence in the Central Valley, California, USA. Hydrogeol. J. 24, 675–684 (2016); erratum 25, 2215–2216 (2017).
72. Belmecheri, S., Babst, F., Wahl, E. R., Stahle, D. W. & Trouet, V. Multi-century evaluation of Sierra Nevada snowpack. *Nat. Clim. Chang.* **6**, 2–3 (2016).
73. Fernando, D. N. et al. What caused the spring intensification and winter demise of the 2011 drought over Texas? *Clim. Dyn.* **47**, 3077–3090 (2016).
74. Haacker, E. M., Kendall, A. D. & Hyndman, D. W. Water level declines in the high plains aquifer: predevelopment to resource senescence. *Ground Water* **54**, 231–242 (2016).
75. Willis, M. J., Melkonian, A. K., Pritchard, M. E. & Ramage, J. M. Ice loss rates at the Northern Patagonian Icefield derived using a decade of satellite remote sensing. *Remote Sens. Environ.* **117**, 184–198 (2012).
76. Chen, J. L., Wilson, C. R., Tapley, B. D., Blankenship, D. D. & Ivins, E. R. Patagonia icefield melting observed by gravity recovery and climate experiment (GRACE). *Geophys. Res. Lett.* **34**, L22501 (2007).
77. Han, S. C., Sauber, J. & Luthcke, S. Regional gravity decrease after the 2010 Maule (Chile) earthquake indicates large-scale mass redistribution. *Geophys. Res. Lett.* **37**, L23307 (2010).
78. Chen, J. L., Wilson, C. R. & Tapley, B. D. The 2009 exceptional Amazon flood and interannual terrestrial water storage change observed by GRACE. *Wat. Resour. Res.* **46**, W12526 (2010).
79. Thomas, A. C., Reager, J. T., Famiglietti, J. S. & Rodell, M. A GRACE-based water storage deficit approach for hydrological drought characterization. *Geophys. Res. Lett.* **41**, 1537–1545 (2014).
80. Getirana, A. C. Extreme water deficit in Brazil detected from space. *J. Hydrometeorol.* **17**, 591–599 (2016).
81. Gaughan, A. E. & Waylen, P. R. Spatial and temporal precipitation variability in the Okavango–Kwando–Zambezi catchment, southern Africa. *J. Arid Environ.* **82**, 19–30 (2012).
82. Andersen, O. B. et al. in *Gravity, Geoid and Earth Observation, International Association of Geodesy Symposia* Vol. 135 (ed. Mertikas, S.) 521–526 (Springer, Berlin, 2010).
83. Swenson, S. & Wahr, J. Monitoring the water balance of Lake Victoria, East Africa, from space. *J. Hydrol.* **370**, 163–176 (2009).
84. Ahmed, M., Sultan, M., Wahr, J. & Yan, E. The use of GRACE data to monitor natural and anthropogenic induced variations in water availability across Africa. *Earth Sci. Rev.* **136**, 289–300 (2014).
85. Ndehedehe, C. E., Awange, J. L., Kuhn, M., Agutu, N. O. & Fukuda, Y. Climate teleconnections influence on West Africa's terrestrial water storage. *Hydrol. Processes* **31**, 3206–3224 (2017).
86. Crowley, J. W., Mitrovica, J. X., Bailey, R. C., Tamisiea, M. E. & Davis, J. L. Land water storage within the Congo Basin inferred from GRACE satellite gravity data. *Geophys. Res. Lett.* **33**, L19402 (2006).
87. Ramillien, G., Frappart, F. & Seoane, L. Application of the regional water mass variations from GRACE satellite gravimetry to large-scale water management in Africa. *Remote Sens.* **6**, 7379–7405 (2014).
88. van Dijk, A. J. M. et al. The Millennium Drought in southeast Australia (2001–2009): natural and human causes and implications for water resources, ecosystems, economy, and society. *Wat. Resour. Res.* **49**, 1040–1057 (2013).
89. Boening, C., Willis, J. K., Landerer, F. W., Nerem, R. S. & Fasullo, J. The 2011 La Niña: so strong, the oceans fell. *Geophys. Res. Lett.* **39**, L19602, (2012).
90. Munier, S., Becker, M., Maisongrande, P. & Cazenave, A. Using GRACE to detect groundwater storage variations: the cases of Canning Basin and Guarani aquifer system. *Int. Water Tech. J.* **2**, 2–13 (2012).
91. Jaramillo, F. & Destouni, G. Local flow regulation and irrigation raise global human water consumption and footprint. *Science* **350**, 1248–1251 (2015).
92. Fietelson, E. in *Water policy in Israel: Context*, Issues *and Options* (ed. Becker, N.) 15–32 (Springer Science & Business media, Dordrecht, 2013).
93. Bhanja, S. N. et al. Groundwater rejuvenation in parts of India influenced by water-policy change implementation. *Sci. Rep.* **7**, 7453 (2017).
94. Eicker, A., Forootan, E., Springer, A., Longuevergne, L. & Kusche, J. Does GRACE see the terrestrial water cycle "intensifying"? *J. Geophys. Res. Atmos.* **121**, 733–745 (2016).
95. Kusche, J., Eicker, A., Forootan, E., Springer, A. & Longuevergne, L. Mapping probabilities of extreme continental water storage changes from space gravimetry. *Geophys. Res. Lett.* **43**, 8026–8034 (2016).
96. Green, T. R. et al. Beneath the surface of global change: impacts of climate change on groundwater. *J. Hydrol.* **405**, 532–560 (2011).
97. Taylor, R. G. et al. Ground water and climate change. *Nat. Clim. Chang.* **3**, 322–329 (2013).
98. Swenson, S. C. & Milly, P. C. D. Climate model biases in seasonality of continental water storage revealed by satellite gravimetry. *Wat. Resour. Res.* **42**, W03201 (2006).
99. McCabe, M. F. et al. The future of Earth observation in hydrology. *Hydrol. Earth Syst. Sci.* **21**, 3879–3914 (2017).
100. Flechtner, F. et al. What can be expected from the GRACE-FO laser ranging interferometer for Earth science applications? *Surv. Geophys.* **37**, 453–470 (2016).

METHODS

GRACE data have traditionally been processed by solving for gravity anomalies in terms of the Stokes coefficients (namely, C_{lm} and S_{lm}, with l denoting degree and m denoting order), which are the coefficients of the spherical harmonic expansion of Earth's gravity field[16,101–106]. These solutions suffer from correlated errors that manifest as longitudinal striping in the gravity solution, which requires tailored 'destriping' and smoothing post-processing filters to remove[107]. Although largely successful in removing errors, the post-processing also damps and smooths real geophysical signals[101]. Recent advances in GRACE data processing have shown that solving for gravity anomalies in terms of mass concentration (mascon) functions with carefully selected regularization results in superior localization of signals on an elliptical Earth[4,21,108,109]. For instance, mascon solutions correlate better with in situ ocean-bottom pressure recorders than spherical-harmonic solutions[21,109], improve the spatial resolution of mass changes in Greenland[29] and were used to detect changes in the Atlantic meridional overturning circulation[110]. Currently, there are three publicly available GRACE mascon solutions: Jet Propulsion Laboratory mascons RL05M.1 version 2[21,111] (JPL-M), Center for Space Research mascons RL05M[109] (CSR-M) and Goddard Space Flight Center mascons version 2.3b[4] (GSFC-M). JPL-M parameterizes the gravity field with 4,551 equal-area 3° mascon elements, whereas CSR-M and GSFC-M both parameterize the gravity field in terms of 1° mascon elements (~41,000 mascon elements are solved for in each solution). Although the implementation details of each mascon solution differ, we note that the JPL-M solution has the unique characteristic that each 3° mascon element is relatively uncorrelated with neighbouring mascon elements, whereas the 1° mascon elements in CSR-M and GSFC-M solutions are highly correlated with their neighbours. Three degrees correspond approximately to the 'native' resolution of GRACE, and the lack of correlation between neighbouring mascon elements in the retrieval allows for a quantitative understanding of leakage errors when aggregating mass anomalies within a hydrological basin[112]—in fact, no literature yet exists on quantifying leakage errors in 1° mascon solutions. Therefore, in this work we use JPL-M for trend analysis and mapping; however, we use all three mascon solutions (JPL-M, CSR-M and GSFC-M) to derive uncertainties.

The JPL-M solution parameterizes each monthly gravity field in terms of 4,551 equal-area, surface spherical-cap mass-concentration functions and uses a regularization approach that implements both spatial and temporal correlations to remove correlated errors during the gravity inversion. A coastline resolution improvement filter is used to separate between land and ocean mass within mascons that span coastlines[112]. Because GRACE does not produce a reliable estimate of Earth's oblateness (C_{20} coefficient), we follow the standard protocol of using satellite laser ranging to provide this estimate[113]. Further, GRACE gravity-field anomalies are measured in the centre-of-mass reference frame of Earth and therefore need to be augmented with a 'geocentre' estimate to capture all surface-mass changes[114]. GIA corrections are made using the updated ICE-6G_D model[64,65], with an exception for Antarctica, for which we reduce the fitted rate of mass change by 9.2 Gt yr^{-1} on the basis of a regional model[115] that potentially provides a better GIA estimate for Antarctica[116]. Finally, corrections are made to the C_{21} and S_{21} coefficients[117] (degree-2 coefficients are related to the moments and products of inertia with respect to a defined reference frame and set of background force models) to fully remove the pole tide from the GRACE data. Jumps in the background atmosphere and ocean dealiasing product are corrected as well[118].

Prior to computing the best-fit linear trend from a TWS time series, the seasonal cycle was removed as follows. First, missing months of data were filled by linear interpolation. Next, the mean monthly seasonal cycle was computed by averaging all Januaries, all Februaries, etc. Finally, for each month in the original, non-gap-filled time series, the mean for the corresponding month of the year was subtracted. The first step (gap filling) was necessary because, for example, the month of May was under-sampled in the second half of the study period, which caused the mean May to be biased in locations where a consistent trend existed (that is, most of the regions of this study).

Trend error estimates account for both systematic and random GRACE measurement errors, as well as the systematic error of the GIA model. The GRACE measurement error is taken to be 1σ, where σ is the standard deviation between trend estimates obtained from JPL-M, CSR-M and GSFC-M. Given the specific basin boundaries used in this study, we find JPL-M to have more pronounced trends (both positive and negative) than CSR-M and GSFC-M, which is consistent with previous conclusions[119]. This spread is due to a fundamental difference in the spectral content between the 3° mascons and 1° mascons, implying that leakage characteristics are different when aggregating mass anomalies over a particular region (somewhat counter-intuitively, the 3° mascons 'focus' more signals than the 1° sampled mascons). In essence, the 'smooth' nature of the 1° mascon solutions (CSR-M and GSFC-M) results in considerable damping of the signal over our regions of interest owing to leakage across the basin boundaries. For a more direct comparison of the three solutions over our regions of interest, we matched the spectral content of JPL-M to that of CSR-M. The regularization of the CSR

mascon solution is based on a smoothed (using a 200-km Gaussian) representation of a regularized spherical-harmonic solution[109]. Hence, it is expected that the final mascon solution will inherit some of these spectral characteristics. Therefore, we smooth JPL-M with a 200-km-radius Gaussian filter and compare the trend estimates of the smoothed version of JPL-M to those of CSR-M and GSFC-M. Thus, the agreement is substantially improved, and trends in the smoothed version of JPL-M are also damped similarly to CSR-M and GSFC-M (see Extended Data Fig. 9 for an example). Similar analysis has been performed before in a study of mass variations over the Caspian Sea[120]. We use the standard deviation of trend estimates obtained from the smoothed version of JPL-M, CSR-M and GSFC-M to derive the GRACE measurement errors. The GIA model error is taken to be the 1σ spread between four competing GIA models[64,65,121–124] that implement two distinct loading histories, four distinct viscosity profiles and different implementations of physics. The uncertainty on the trend for any region is given by the root sum of squares combining the GIA model error (which manifests only as a trend) and the GRACE measurement error.

Time series for the Aral and Caspian seas (regions 17 and 18) were calculated by applying a set of gain factors to the GRACE data. Gain factors redistribute mass within each individual mascon (at sub-mascon resolution), allowing exact averaging kernels to be applied to a region of interest and retrieval of accurate, unbiased (by leakage) mass-change values[101,112]. These particular gain factors were derived[112] using a combination of total-column soil moisture output from the Noah land-surface model driven by the Global Land Data Assimilation System[125] (which does not include sea-water variations) along with altimetry data[126] over the Aral and Caspian seas.

Recent variations in Caspian Sea level have been attributed by previous studies to natural meteorological variability[8] and direct evaporation from the sea surface[61]. We tested these two theories as well as a third, agricultural water consumption. Flow in the Volga River, which delivers roughly 80% of the runoff to the Caspian Sea, is controlled by a series of eleven dams[127]. Among other purposes, these ensure a steady supply of water for crop irrigation[127]. No data were available to quantify interannual variations in irrigation extent, intensity or volumes in the Caspian Sea drainage basin during the study period. Estimates of Russian annual wheat, maize, rice and soybean production[128] (in tonnes) during 1992–2015 were obtained from the Organisation for Economic Co-operation and Development (OECD). According to the irrigation dataset[23], the Volga River basin, which drains to the Caspian Sea, includes 3% irrigated crops and 37% rain-fed crops by area, and it accounts for about half of all Russian crop production. Therefore, Russian crop production is a fair, but imperfect, indicator of agricultural water demand in the basin. Yearly total production was normalized by subtracting the 24-year mean and dividing it by the standard deviation. Normalization was similarly performed on the annual time series of GPCP precipitation[22] over the Caspian Sea and Volga River drainage basins, the Volga River discharge, reanalysis-based Caspian Sea evaporation[129] and changes in Caspian Sea level obtained from satellite altimetry[24]. Correlation coefficients (and significance levels) between normalized Caspian Sea level change and its significant drivers (Extended Data Fig. 10) were 0.78 (Volga River discharge; $P < 0.001$), -0.47 (crop production; $P = 0.02$), -0.43 (Caspian Sea evaporation; $P = 0.04$) and 0.41 (Caspian Sea drainage basin precipitation; $P = 0.05$). Correlation coefficients (and significance levels) between normalized Volga River discharge and significant drivers were 0.52 (Volga River basin precipitation; $P = 0.01$) and -0.40 (crop production; $P = 0.06$). Notably, the correlation between crop production and precipitation was negligible, suggesting that irrigation effectively mitigates the impact of drought. Interannual variations in Caspian Sea evaporation do indeed contribute significantly to Caspian Sea level changes. However, annual Volga River discharge variations are better correlated with annual changes in Caspian Sea level, they are larger than variations in Caspian Sea evaporation (standard deviation of 48 Gt versus 18 Gt, compared with a mean magnitude of annual Caspian Sea level change of 38 Gt) and they are controlled by both precipitation and rising agricultural water demand[127]. We therefore conclude that all three factors contributed to the observed water loss (-23.7 ± 4.2 Gt yr^{-1} from GRACE, ignoring steric effects; -25.4 Gt yr^{-1} from satellite altimetry) during 2002–2015.

For the Gulf of Alaska coast and the Patagonian ice fields (regions 3 and 23), it was also necessary to increase the rates of mass loss (by 7 Gt yr^{-1} and 9 Gt yr^{-1}, respectively) to account for Little Ice Age GIA[31]. We note that the full GIA corrections to Antarctica, the Gulf of Alaska coast and the Patagonian ice fields are not incorporated into Extended Data Fig. 1 and 3.

The irrigated area fractions (Table 1) were computed by area-weighted averaging of the individual pixel values of irrigation intensity[23] (%) within each study region. Precipitation trends (mm yr^{-1}) were computed on the basis of monthly data[22], as above for TWS, except that there were no gaps to fill. Precipitation trends (% per year) and percentages of normal precipitation were computed using the 1979–2015 annual mean precipitation totals for each region. Predicted precipitation changes were computed as area-weighted averages from the IPCC dataset[25] over the study

regions. The precipitation maps in Fig. 2 were computed as above, but on a pixel-by-pixel basis.

The explanation for the mass-loss trend in northwestern China (region 11), -5.5 ± 0.5 Gt yr^{-1}, is complex. Drought was not a factor, given that precipitation was 10% above normal and stable during the period. Two recent studies[130,131] estimated the rate of glacier loss over the entire Tien Shan mountain range to be -5.4 ± 2.9 Gt yr^{-1} and -7.5 ± 3.4 Gt yr^{-1} based on Ice, Cloud and Land Elevation Satellite (ICESat) observations from 2003 to 2009. These estimates are somewhat smaller than our GRACE-based estimate of TWS decline in region 11 during that period (-8.3 ± 0.8 Gt yr^{-1}), despite region 11 encompassing less than half of the area of glacier melt[130]. Hence, we conjecture that an additional catalyst for mass loss must exist. Xinjiang province is one of the world's largest producers of coal, having an estimated 2.2 trillion tons of reserves[132]. Reported rates of coal removal and burning are more than an order of magnitude smaller than the GRACE-observed mass loss[132], but mining involves dewatering of the aquifers that the mines intersect. Consequent groundwater depletion in the area is possible[52] but unconfirmed. Adding to the complexity, region 11 lies within a larger endorheic basin, which means that water pumped from the ground or melting from glaciers will remain as surface water, become groundwater recharge or evapotranspire, as opposed to flowing to the ocean. However, on the basis of satellite altimetry data, the elevations of the five lakes within the surrounding endorheic basin did not increase during the study period. All either declined or did not change significantly. The two lowlands into which region 11 drains (one to the northwest, one to the southeast) have GRACE-based trends of 0.3 Gt yr^{-1} and -0.6 Gt yr^{-1} (both insignificant). Ultimately, evapotranspiration must account for the water lost from region 11. The average annual precipitation in region 11 is 194 mm yr^{-1}, making it the fourth-driest of the 32 study regions. The endorheic basin is extensively irrigated, including 7% of region 11, and irrigation intensity is likely rising in support of Xinjiang province's population growth (from 18.2 million in 2000 to 21.8 million in 2010)[51]. Massive amounts of surface water from Lake Bosten and the Kongque River (both to the southeast of region 11) are transferred via aqueducts southwards to the Tarim River to support farming in the arid plains; however, the Tarim River runs dry before reaching its natural terminus, Lop Nor lake[50]. To summarize, the Tien Shan mountain glaciers in region 11 are shrinking because of global warming. Groundwater may be declining owing to agricultural withdrawals or mining operations, but the latter is unconfirmed. Because region 11 lies within an endorheic basin, neither glacier melt nor groundwater pumping can alone explain the observed TWS depletion. The corollary is that the resulting additions to surface water are balanced by desert- and irrigation-enhanced evapotranspiration.

As noted in the main text, although previous GRACE-based studies of the North China Plain (region 12) agreed that groundwater depletion associated with intense irrigation was the cause of the trend, they offered a wide range of estimates of the TWS or groundwater trend. Specifically, these estimates were -8.3 Gt yr^{-1} over a 370,000-km^2 area[133], -35 Gt yr^{-1} over a 2,086,000-km^2 area[134], -2.33 Gt yr^{-1} over a 370,000-km^2 area[135] and -14.09 Gt yr^{-1} over a 1,500,000-km^2 area[136], compared with our estimate of -11.3 Gt yr^{-1} over an 876,004-km^2 area.

Data availability. Specific sources of data used in this study were the following. The primary GRACE TWS dataset is JPL Mascon RL05M.1 version 2, accessed on 3 February 2017 from https://grace.jpl.nasa.gov/data/get-data/jpl_global_mascons/. Additional GRACE TWS datasets used to estimate errors were CSR RL05 Mascon version 1, accessed on 20 September 2017 from http://www2.csr.utexas.edu/grace/RL05_mascons.html, and GSFC Mascon version 2.3b, accessed on 5 October 2017 from https://neptune.gsfc.nasa.gov/gngphys/index.php?section=413. Primary GIA data used in this study were the ICE-6GD model, accessed on 1 December 2017 from http://www.atmosp.physics.utoronto.ca/~peltier/data.php, and the IJ05_R2 GIA correction for Antarctica, accessed on 3 February 2018 from http://onlinelibrary.wiley.com/doi/10.1002/jgrb.50208/full. Additional GIA data used to compute the GIA model error included ICE-6G_ANU_D, accessed on 3 February 2018 from http://onlinelibrary.wiley.com/doi/10.1002/2017JB014930/full, the A et al. (2013)[121] GIA model, accessed on 16 December 2013 from ftp://podaac-ftp.jpl.nasa.gov/allData/tellus/L3/pgr/, and the Paulson et al. (2007)[122] GIA model, accessed on 3 February 2018 from https://academic.oup.com/gji/article/171/2/497/2018541. Atmosphere and ocean dealiasing product jump corrections were accessed on 13 June 2016 from ftp://podaac-ftp.jpl.nasa.gov/allData/grace/docs/. Precipitation data from GPCP version 2.3 were accessed on 23 September 2016 from https://www.esrl.noaa.gov/psd/data/gridded/data.gpcp.html. Global rain-fed, irrigated and paddy croplands version-1 data were accessed on 12 September 2016 from http://ftp-earth.bu.edu/public/friedl/GRIPCmap/. Global reservoir/lake elevation TPJO.2.3 data were accessed on 29 July 2016 from https://ipad.fas.usda.gov/cropexplorer/global_reservoir/. Precipitation change data predicted by the IPCC 5th Assessment Report (RCP8.5) were accessed on 1 September 2016 from https://www.ipcc.ch/pdf/assessment-report/ar5/wg1/WG1AR5_AnnexI_FINAL.pdf. Russian crop production data were accessed on 16 August 2017 from https://data.oecd.org/agroutput/crop-production.htm. Latent heat flux (evapotranspiration) data for the Caspian Sea and its drainage basin were extracted from MERRA-2 version M2TMNXLND_5.12.4, accessed on 19 September 2017 from https://disc.sci.gsfc.nasa.gov/datasets/M2TMNXLND_5.12.4/summary. Volga River discharge observations are restricted from public access, but a time series of normalized annual discharge values was provided to M.R. by V. Khan of the Hydrometeorological Research Center of the Russian Federation.

The JPL RL05M GRACE solution used in this study is identical to that available from the NASA/JPL GRACE Tellus website, with the exception that we implemented a different GIA model, a correction to the pole tide and corrections to the background atmosphere and ocean dealiasing model. These adjustments are available from D.N.W. upon request. Data analysed to create Extended Data Fig. 9 are available from D.N.R. upon request. Excel spreadsheets containing the data and calculations used to create Table 1 and Extended Data Fig. 10 are available from M.R. upon request.

Code availability. MATLAB scripts were used to prepare GRACE-based TWS time series for the study regions, including GIA adjustments, C_{21} and S_{21} coefficient replacements, and corrections for jumps in the atmosphere and ocean dealiasing products. These are available from D.N.W. upon reasonable request. TWS time series analyses, including trend estimation and r^2 computation, were performed within Excel spreadsheets, which are available from M.R. upon reasonable request.

101. Landerer, F. W. & Swenson, S. C. Accuracy of scaled GRACE terrestrial water storage estimates. *Wat. Resour. Res.* **48**, W04531 (2012).
102. Dahle, C. et al. in *Observation of the System Earth from Space-CHAMP, GRACE, GOCE and Future Missions* (eds Flechtner, F. et al.) 29–39 (Springer, Berlin, 2014).
103. Mayer-Gürr, T. et al. *ITSG-Grace2016 - Monthly and Daily Gravity Field Solutions from GRACE* https://doi.org/10.5880/icgem.2016.007 (2016).
104. Bruinsma, S., Lemoine, J.-M., Biancale, R. & Vales, N. CNES/GRGS 10-day gravity field models (release 02) and their evaluation. *Adv. Space Res.* **45**, 587–601 (2010).
105. Kurtenbach, E. et al. Improved daily GRACE gravity field solutions using a Kalman smoother. *J. Geodyn.* **59-60**, 39–48 (2012).
106. Liu, X. et al. DEOS Mass Transport model (DMT-1) based on GRACE satellite data: methodology and validation. *Geophys. J. Int.* **181**, 769–788 (2010).
107. Swenson, S. & Wahr, J. Post-processing removal of correlated errors in GRACE data. *Geophys. Res. Lett.* **33**, L08402 (2006).
108. Andrews, S. B., Moore, P. & King, M. A. Mass change from GRACE: a simulated comparison of Level-1B analysis techniques. *Geophys. J. Int.* **200**, 503–518 (2014).
109. Save, H., Bettadpur, S. & Tapley, B. D. High resolution CSR GRACE RL05 mascons. *J. Geophys. Res. Solid Earth* **121**, 7547–7569 (2016).
110. Landerer, F. W., Wiese, D. N., Bentel, K., Boening, C. & Watkins, M. M. North Atlantic meridional overturning circulation variations from GRACE ocean bottom pressure anomalies. *Geophys. Res. Lett.* **42**, 8114–8121 (2015).
111. Wiese, D. N., Yuan, D.-N., Boening, C., Landerer, F. W. & Watkins, M. M. *JPL GRACE Mascon Ocean, Ice, and Hydrology Equivalent Water Height RL05M.1 CRI Filtered Version 2 PO.DAAC, CA, USA* https://doi.org/10.5067/TEMSC-2LCR5 (2016).
112. Wiese, D. N., Landerer, F. W. & Watkins, M. M. Quantifying and reducing leakage errors in the JPL RL05M GRACE mascon solution. *Wat. Resour. Res.* **52**, 7490–7502 (2016).
113. Cheng, M. & Tapley, B. D. Variations in the Earth's oblateness during the past 28 years. *J. Geophys. Res.* **109**, B09402 (2004).
114. Swenson, S., Chambers, D. & Wahr, J. Estimating geocenter variations from a combination of GRACE and ocean model output. *J. Geophys. Res.* **113**, B08410 (2008).
115. Ivins, E. R. et al. Antarctic contribution to sea level rise observed by GRACE with improved GIA correction. *J. Geophys. Res.* **118**, 3126–3141 (2013).
116. Shepherd, A. et al. A reconciled estimate of ice-sheet mass balance. *Science* **338**, 1183–1189 (2012).
117. Wahr, J., Nerem, R. S. & Bettadpur, S. V. The pole tide and its effect on GRACE time variable gravity measurements: Implications for estimates of surface mass variations. *J. Geophys. Res. Solid Earth* **120**, 4597–4615 (2015).
118. Fagiolini, E., Flechtner, F., Horwath, M. & Dobslaw, H. Correction of inconsistencies in ECMWF's operational analysis data during the de- aliasing of GRACE gravity models. *Geophys. J. Int.* **202**, 2150–2158 (2015).
119. Scanlon, B. R. et al. Global evaluation of new GRACE mascon products for hydrologic applications. *Water Resourc. Res.* **52**, 9412–9429 (2016).
120. Chen, J. L., Wilson, C. R., Tapley, B. D., Save, H. & Cretaux, J.-F. Long-term and seasonal Caspian Sea level change from satellite gravity and altimeter measurements. *J. Geophys. Res. Solid Earth* **122**, 2274–2290 (2017).
121. A, G., Wahr, J. & Zhong, S. Computations of the viscoelastic response of a 3-D compressible Earth to surface loading: an application to Glacial Isostatic Adjustment in Antarctica and Canada. *Geophys. J. Int.* **192**, 557–572 (2013).
122. Paulson, A., Zhong, S. & Wahr, J. Inference of mantle viscosity from GRACE and relative sea level data. *Geophys. J. Int.* **171**, 497–508 (2007).
123. Purcell, A., Tregoning, P. & Dehecq, A. An assessment of the *ICE6G_C(VM5a)* glacial isostatic adjustment model. *J. Geophys. Res. Solid Earth* **121**, 3939–3950 (2016).

124. Purcell, A., Tregoning, P. & Dehecq, A. Reply to comment by W. R. Peltier, D. F. Argus, and R. Drummond on "An assessment of the ICE6G_C (VM5a) glacial isostatic adjustment model". *J. Geophys. Res. Solid Earth* **123**, 2029–2032 (2017).
125. Rodell, M. et al. The global land data assimilation system. *Bull. Am. Meteorol. Soc.* **85**, 381–394 (2004).
126. Crétaux, J.-F. et al. SOLS: a lake database to monitor in the near real time water level and storage variations from remote sensing data. *Adv. Space Res.* **47**, 1497–1507 (2011).
127. Avakyan, A. B. Volga-Kama cascade reservoirs and their optimal use. Lakes Reservoirs: Res. *Manage.* **3**, 113–121 (1998).
128. OECD. *Crop Production (Indicator)* https://data.oecd.org/agroutput/crop-production.htm (2017).
129. Gelaro, R. et al. The modern-era retrospective analysis for research and applications, version 2 (MERRA-2). *J. Clim.* **30**, 5419–5454 (2017).
130. Farinotti, D. et al. Substantial glacier mass loss in the Tien Shan over the past 50 years. *Nat. Geosci.* **8**, 716–722 (2015).
131. Gardner, A. et al. A reconciled estimate of glacier contributions to sea level rise: 2003 to 2009. *Science* **340**, 852–857 (2013).
132. Mou, D. & Li, Z. A spatial analysis of China's coal flow. *Energy Policy* **48**, 358–368 (2012).
133. Feng, W. et al. Evaluation of groundwater depletion in North China using the Gravity Recovery and Climate Experiment (GRACE) data and ground-based measurements. *Wat. Resour. Res.* **49**, 2110–2118 (2013).
134. Moiwo, J. P., Tao, F. & Lu, W. Analysis of satellite-based and in situ hydro-climatic data depicts water storage depletion in North China Region. *Hydrol. Processes* **27**, 1011–1020 (2013).
135. Tang, Q., Zhang, X. & Tang, Y. Anthropogenic impacts on mass change in North China. *Geophys. Res. Lett.* **40**, 3924–3928 (2013).
136. Ebead, B., Ahmed, M., Niu, Z. & Huang, N. Quantifying the anthropogenic impact on groundwater resources of North China using Gravity Recovery and Climate Experiment data and land surface models. *J. Appl. Remote Sens.* **11**, 026029 (2017).
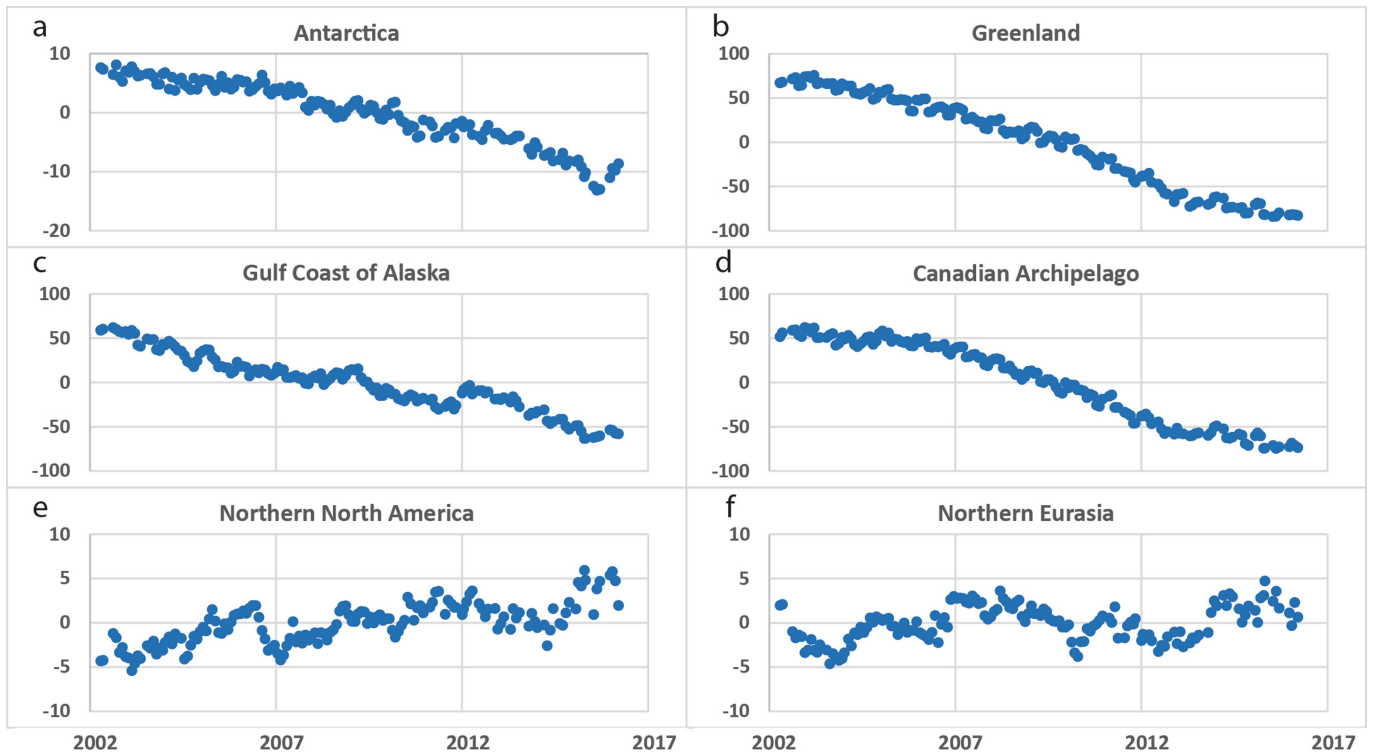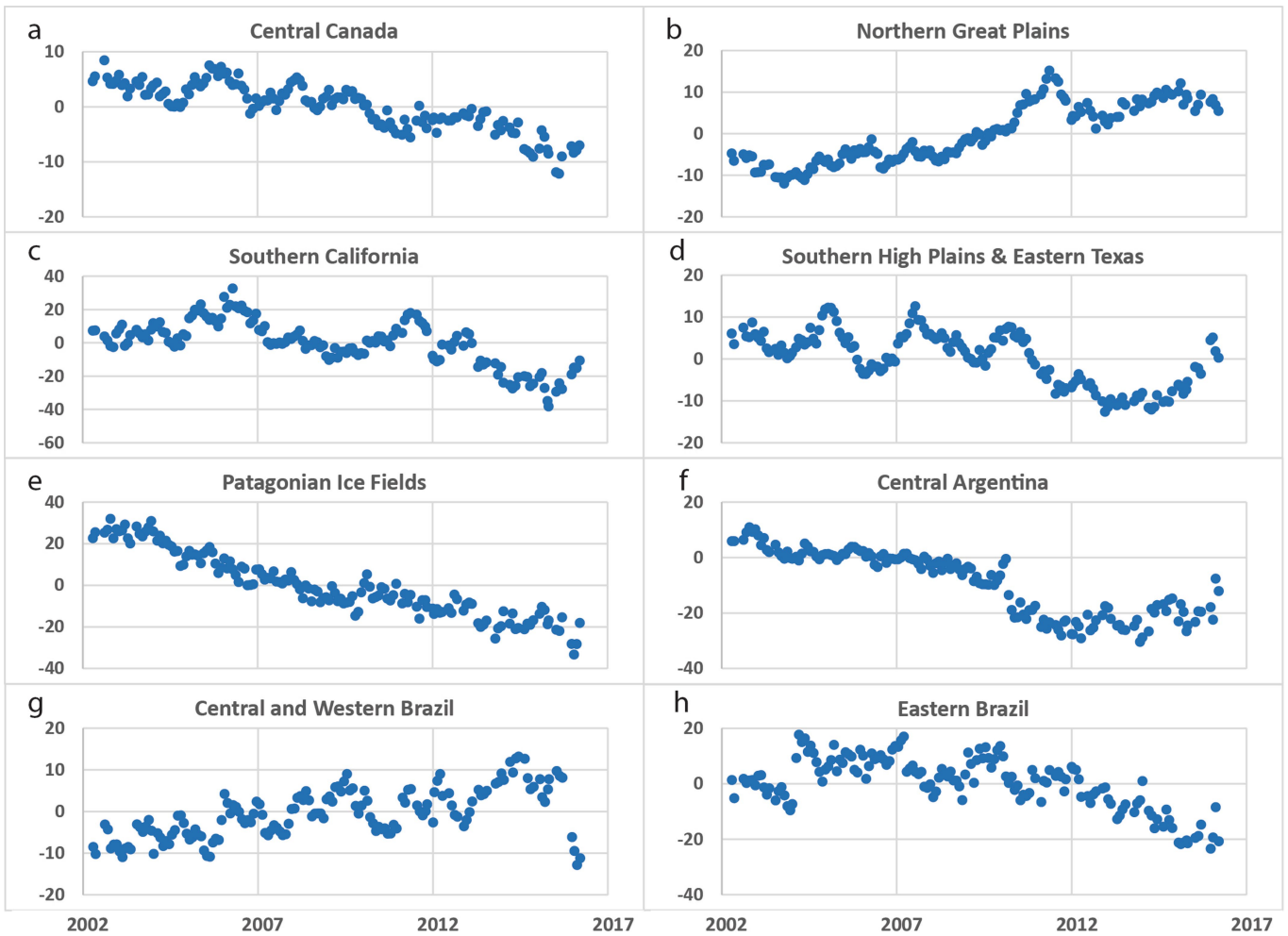
Extended Data Fig. 1 | Non-seasonal TWS anomalies—global regions.
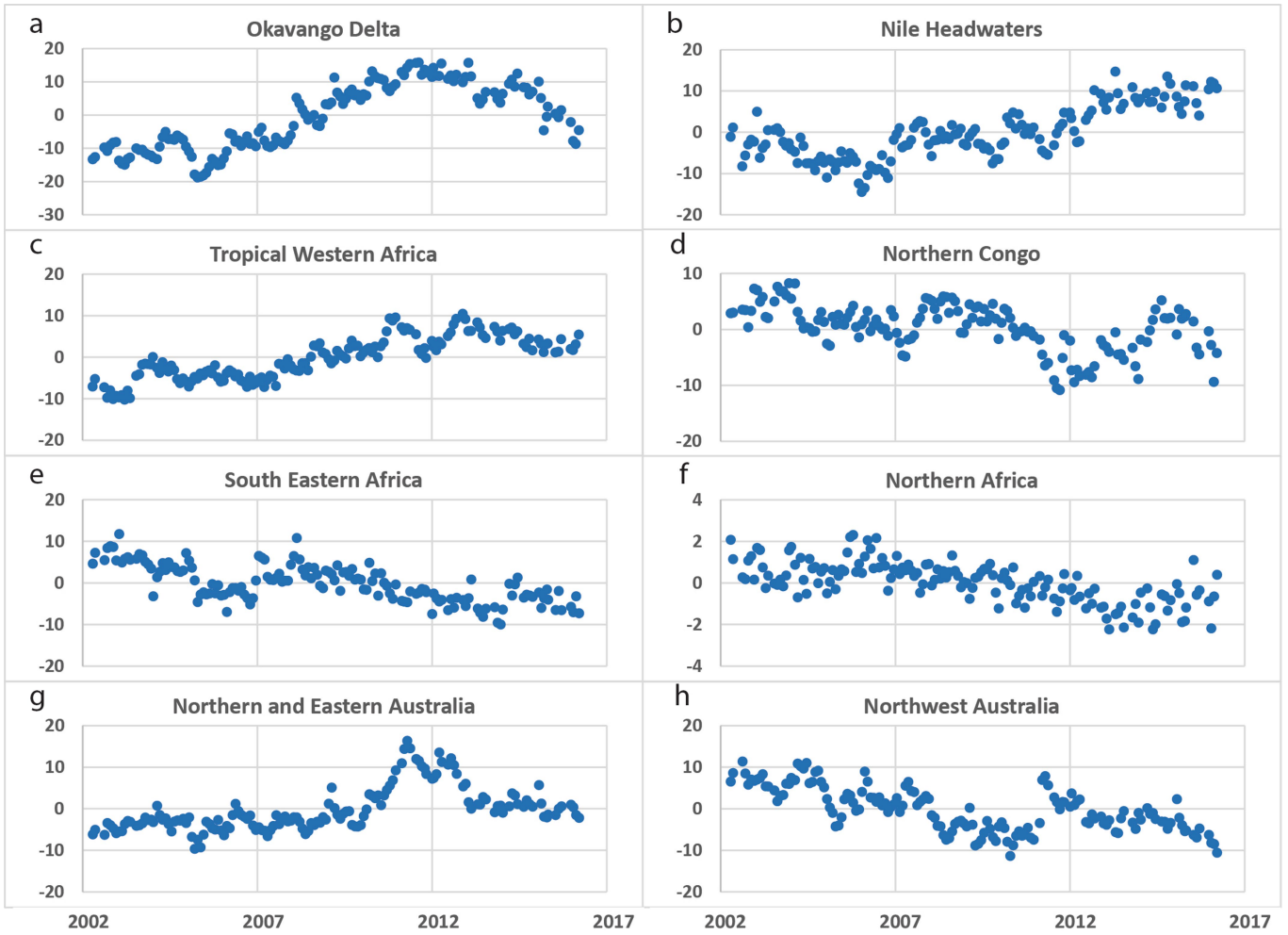**a**–**f**, Time series of monthly TWS anomalies (departures from the period mean) from GRACE, after removing the mean seasonal cycle, averaged over each of study regions 1–6, expressed as equivalent heights of liquid water (in centimetres). We note that the y axes vary among panels.
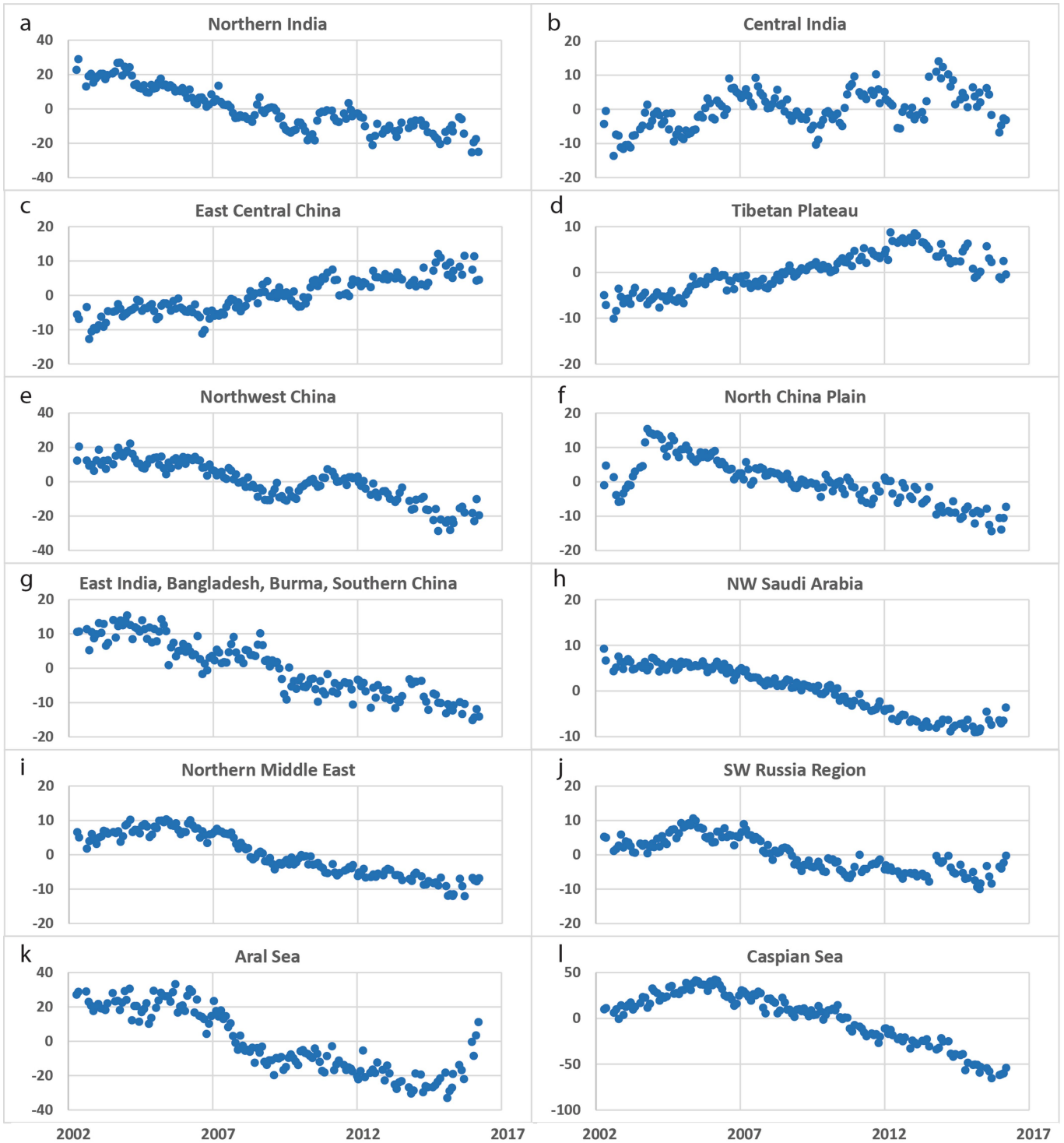
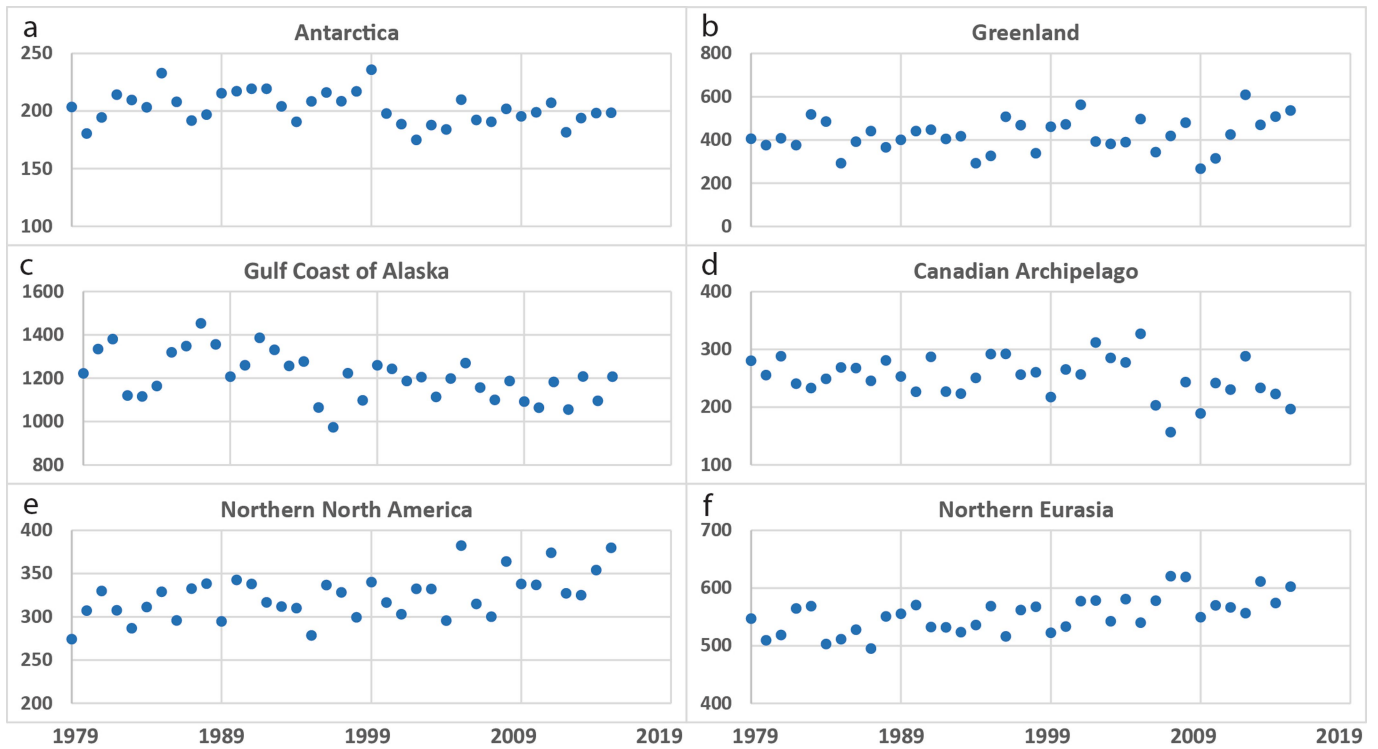**Extended Data Fig. 2 | Non-seasonal TWS anomalies—Eurasia. a–l,** As in Extended Data Fig. 1, for regions 7–18.

Extended Data Fig. 3 | Non-seasonal TWS anomalies—North and South America. a–h, As in Extended Data Fig. 1, for regions 19–26.
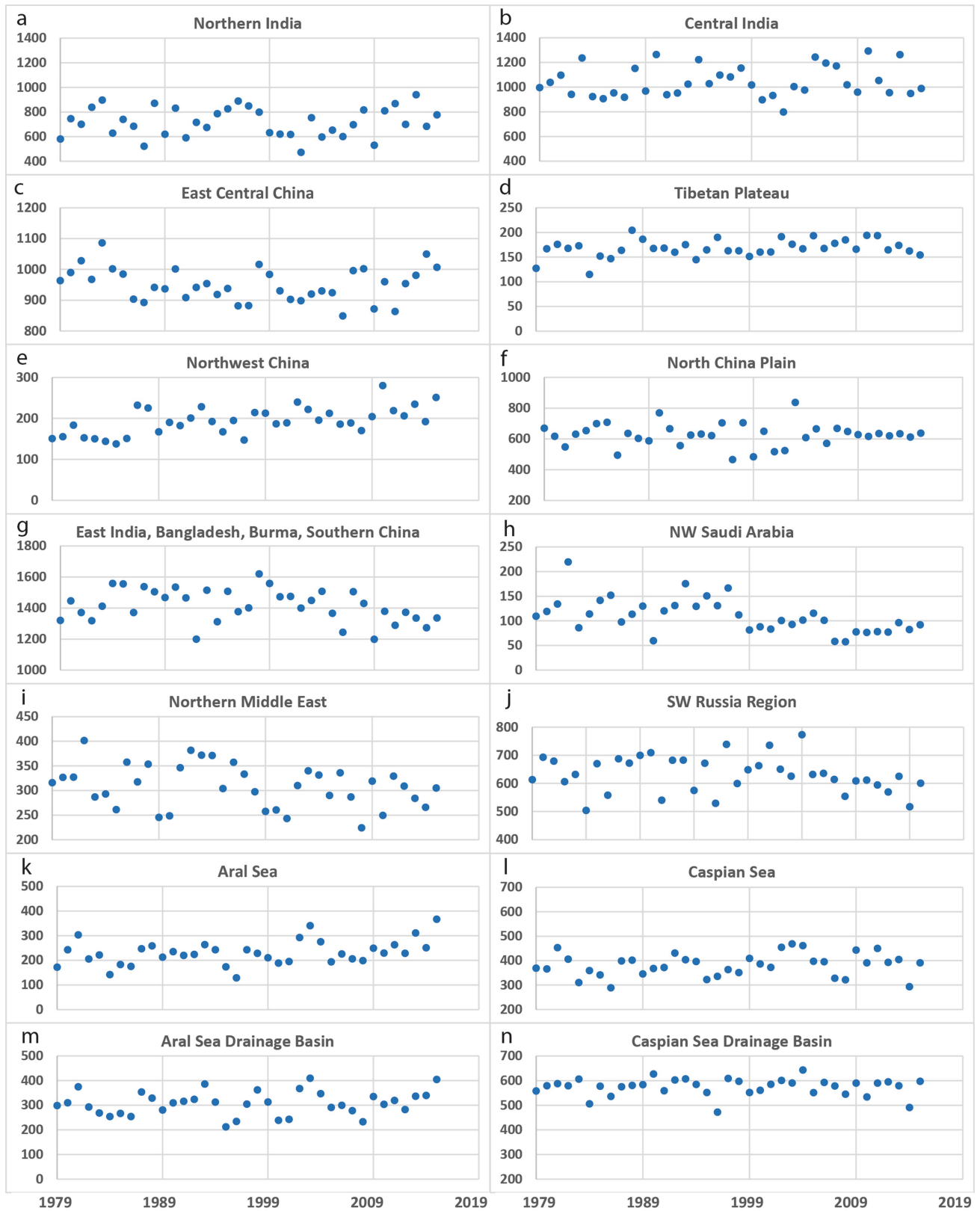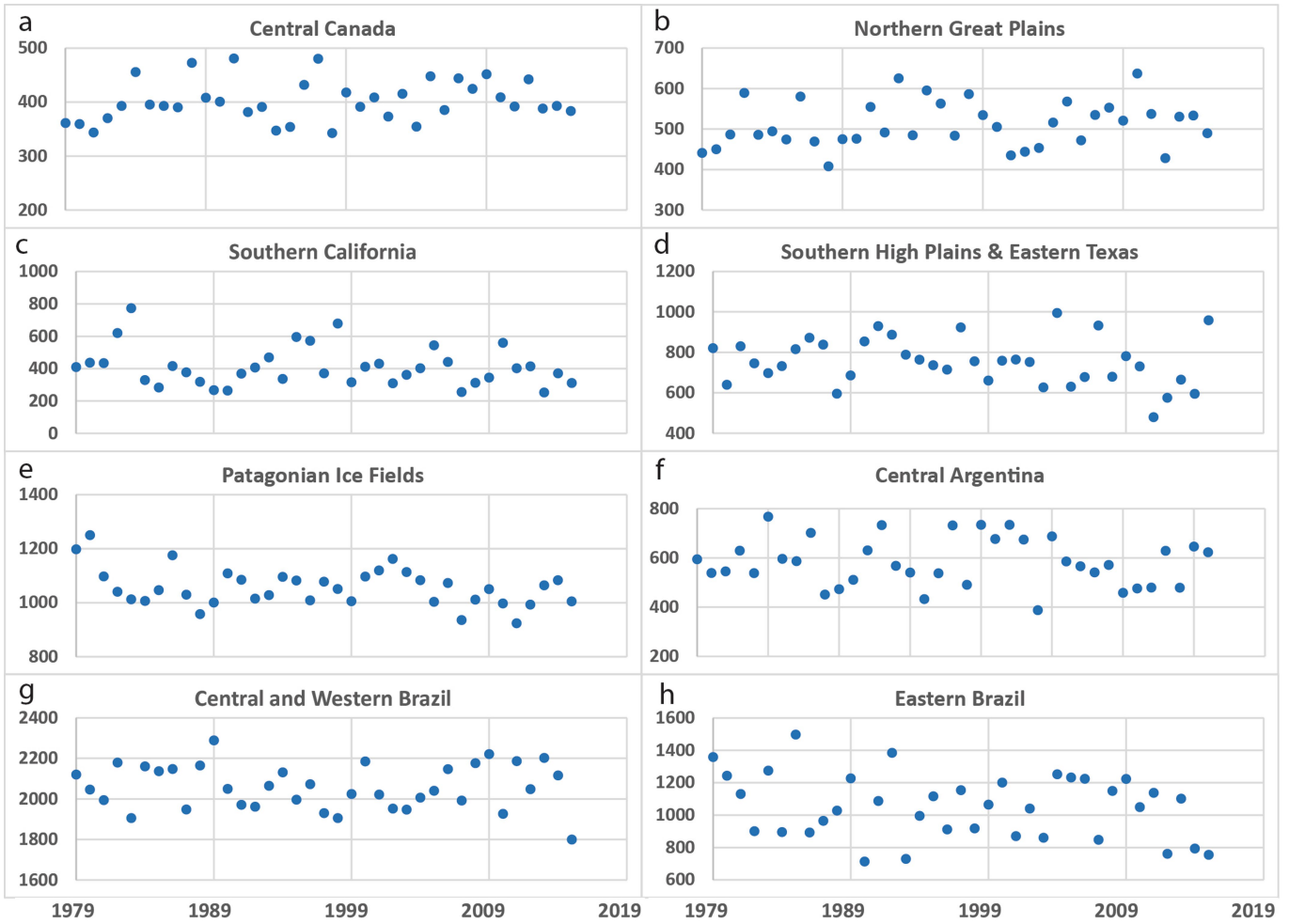
Extended Data Fig. 5 | Annual precipitation totals—global regions.
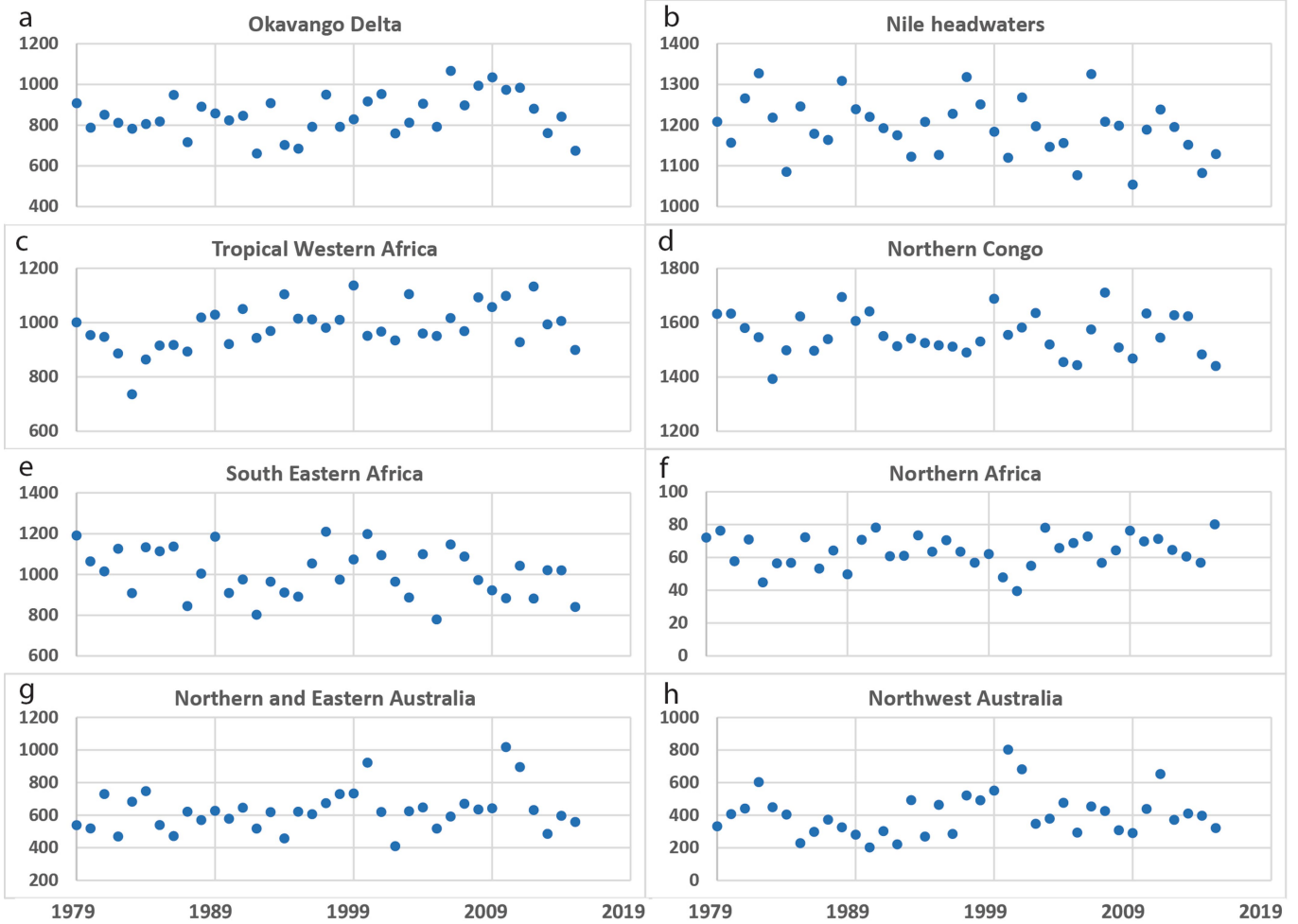**a–f**, Time series of annual precipitation totals (in millimetres) averaged over each of study regions 1–6, based on GPCP v.2.3. We note that the *y* axes vary among panels.

Extended Data Fig. 6 | Annual precipitation totals—Eurasia. a–n, As in Extended Data Fig. 5, for regions 7–18 and the full drainage basins of the Aral and Caspian seas.

Extended Data Fig. 7 | Annual precipitation totals—North and South America. a–h, As in Extended Data Fig. 5, for regions 19–26.

Extended Data Fig. 8 | Annual precipitation totals—Africa and Australia. a–h, As in Extended Data Fig. 5, for regions 27–34.
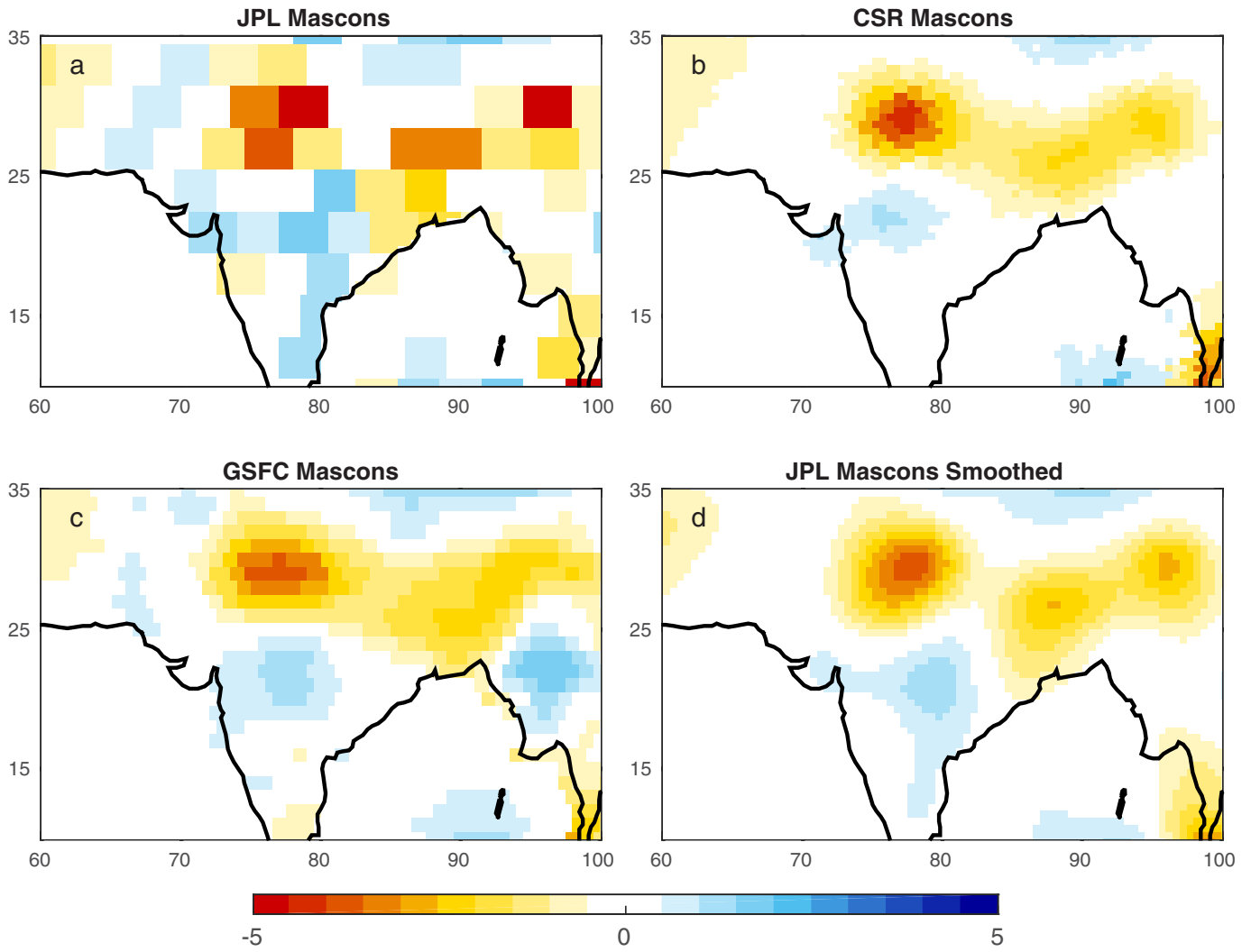
Extended Data Fig. 9 | Comparison of TWS trends (in centimetres per year) over India (January 2003 – March 2016) from three GRACE mascon solutions. a–d, JPL-M 3° (**a**), CSR-M 1° (**b**), GSFC-M 1° (**c**) and JPL-M smoothed with a 200-km-radius Gaussian filter and plotted at 1° (**d**). We note the similarity between **b**–**d**, whose regional trend amplitudes have all been dampened by smoothing.
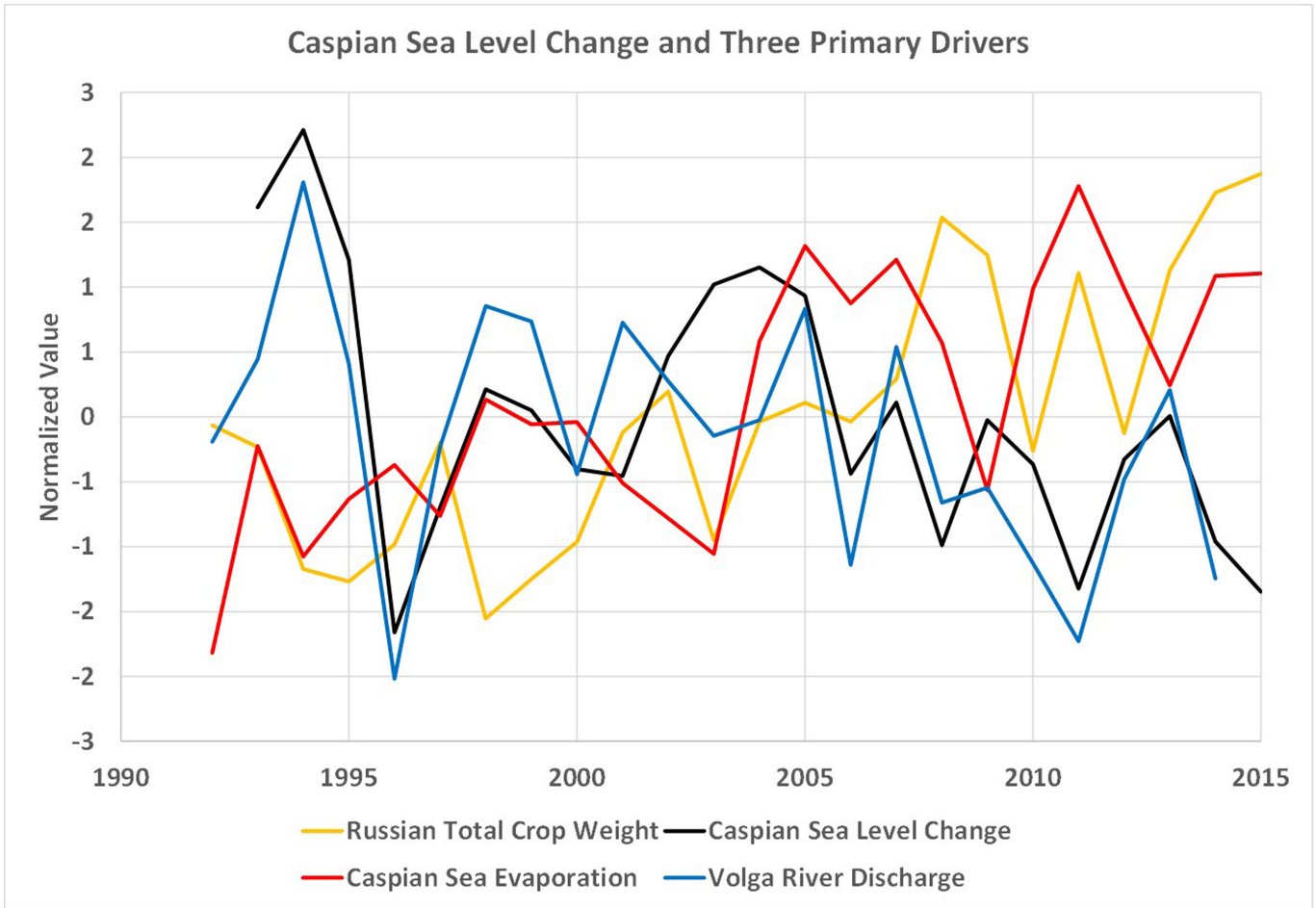
Extended Data Fig. 10 | Comparison of normalized anomalies of Caspian Sea level changes and three primary drivers. Normalized anomalies of changes in annual mean Caspian Sea level (black), Volga River discharge (blue), Russian total crop weight (yellow) and Caspian Sea evaporation (red). Precipitation (Extended Data Fig. 6) is the other primary driver. Sea-level change is positively correlated with Volga River discharge and negatively correlated with Russian crop weight and evaporation.